TESTING OF A DUCTED AXIAL FLOW TIDAL TURBINE

By

Thomas A. Lokocz

B.S University of Maine, 2010

A THESIS

Submitted in Partial Fulfillment of the

Requirements for the Degree of

Masters of Science

(in Mechanical Engineering)

The Graduate School

University of Maine

August, 2012

Advisory Committee:

Michael Peterson Jr., PhD, Libra Foundation Professor of Mechanical Engineering, Advisor

Richard Kimball, PhD, Associate Professor, Maine Maritime Academy

Krish P Thiagarajan, PhD, Correll Presidential Chair in Energy and Professor of Mechanical Engineering

LIBRARY RIGHTS STATEMENT

In presenting this thesis in partial fulfillment of the requirements for an advanced degree at the University of Maine, I agree that the Library shall make it freely available for inspection. I further agree that permission for “fair use” copying of this thesis for scholarly purposes may be granted by the Librarian. It is understood that any copying or publication of this thesis for financial gain shall not be allowed without my written permission.

Signature:

Date:

TESTING OF A DUCTED AXIAL FLOW

TIDAL TURBINE

By: Thomas A. Lokocz

Thesis Advisor: Dr. Michael Peterson

An Abstract of the Thesis Presented
in Partial Fulfillment of the Requirements for the
Degree of Master of Science
(in Mechanical Engineering)
August, 2012

Energy independence and a reduction on the reliance on fossil fuels is a critical area of current research and development. Utilizing the energy in the world's oceans can help the world move towards a more sustainable energy supply. One of the most promising sources of ocean energy is tidal energy or marine hydrokinetics, the topic of this thesis.

This research analyzes the performance of a ducted axial flow tidal turbine and compares the result to an unducted turbine. While the focus of this research is on experimental results obtained in tow tank tests, the turbine and duct were designed using the open source software code, OpenProp. OpenProp was used because of the suitability of the design approach for the optimization of a turbine design and its modeling capability for ducted propellers. While OpenProp has the capability to analyze ducted turbines this capability has been added only recently and has not been validated. Thus the duct used in the experimental work could not be optimized and was intended to provide data which could be used as a part of the validation of the ducted portion of the

code. Literature reviews indicate that limited experimental data exists for the performance of comparable ducted and unducted turbines.

The design used is a three-bladed, ducted turbine with blade shapes optimized in OpenProp. For the unducted case, an optimal C_p of 0.44 was measured at a tip speed ratio of 4.43. The duct was shown to have a detrimental effect on the performance of the turbine with a maximum $C_p = .4$ at a tip speed ratio of 4.4. This result demonstrates the challenges associated with the design of an efficient ducted turbine

THESIS ACCEPTANCE STATEMENT

On behalf of the Graduate Committee for Thomas A. Lokocz I affirm that this manuscript is the final and accepted thesis. Signatures of all committee members are on file with the Graduate School at the University of Maine, 42 Stodder Hall, Orono, Maine.

Dr. Michael Peterson Jr., Professor of Mechanical Engineering, Date

ACKNOWLEDGEMENTS

There are many people who made this thesis possible. I would like to thank my wife, Claire and son, Cabot for their patience and support. I would also like to thank my advisors Dr. Michael "Mick" Peterson and Dr. Richard Kimball for their guidance, insight and editing. Thank you to Dr. Brenden Epps whose experience and advice were always valuable.

This thesis would not be possible without the support of my fellow graduate students who helped in the lab and data processing, especially: Geoffrey deBree for data processing, Matthew Cameron for help with the tow tank, Raul Urbina for numerical modeling and writing advice, and Melissa Colleen Swanger for being a good lab mate. I would also like to thank the following undergraduate students for help with fabrication, testing and coding: Samuel Sayen for machining, Tom McKay for testing and James Staszko for both testing and creating figures.

Finally, I would like to thank the University of Maine, Department of Mechanical Engineering and the U.S. Department of Energy (grant EE-000298) for their financial support to make this project possible.

TABLE OF CONTENTS

ACKNOWLEDGEMENTS iii

LIST OF TABLES viii

LIST OF FIGURES ix

NOMENCLATURE xii

PERFORMANCE EQUATIONS xiii

CHAPTER 1. INTRODUCTION 1

1.1 Motivation 1

1.2 Background 2

1.2.1 OpenProp 3

1.2.2 Free Tip Turbines 4

1.2.3 Ducted Turbines 4

1.3 Thesis Overview 4

CHAPTER 2. TURBINE DESIGN AND FABRICATON 5

2.1 Free Tip Turbine Design 6

2.2 Ducted Turbine Design 7

2.2.1 Duct Geometry 8

2.3 Turbine Fabrication 9

CHAPTER 3. EXPERIMENTAL TESTING 11

3.1 Experimental Setup 11

3.1.1 Tow Tank 11

3.1.2 Axial Flow Turbine Test Platform 12

3.1.3 Measured Quantities 14

3.1.3.1 Torque 15

3.1.3.2 Rotor Thrust 16

3.1.3.3 Duct Thrust 16

3.1.3.4 Turbine Frequency 18

3.1.3.5 Inflow Velocity 18

3.2 Test Methods 19

3.2.1 Calibration 19

3.2.1.1 Torque Calibration 19

3.2.1.2 Rotor Thrust Calibration 21

3.2.1.3 Duct thrust Calibration 22

3.2.2 Turbine Test Procedure 22

CHAPTER 4. DATA PROCESSING 24

4.1 Filtering 24

CHAPTER 5. RESULTS 27

5.1 Free Tip Results 27

5.1.1 Free Tip C_P 28

5.1.2 Free Tip C_T 29

5.2 Ducted Results.....29

5.2.1 Ducted C_P 30

5.2.2 Ducted C_T 30

5.2.3 Duct Thrust Coefficient 31

5.2.4 Ducted Turbine Rotor Without Duct 32

5.2.4.1 C_P For Ducted Turbine Rotor Without Duct 32

5.2.4.2 C_T For Ducted Turbine Without Duct 33

CHAPTER 6. DISCUSION AND CONCLUSIONS 34

6.1 Discussion 34

6.1.1 Reynolds Number and Water Temperature Effects.....36

6.1.1.1 Free tip turbine.....37

6.1.1.2 Ducted Turbine 38

6.1.2 Duct Thrust 38

6.1.3 OpenProp Validation 41

6.1.4 Free Tip and Ducted C_T Discussion 42

6.2 Conclusions 44

6.3 Future Work 46

6.3.1 Experimental.....46

6.3.2 Modeling.....47

WORKS CITED 48

APPENDIX A: Free tip input code 51

APPENDIX B: Free tip blade Geometry file 55

APPENDIX C: Ducted input code 56

APPENDIX D: Ducted Blade Geometry File 58

APPENDIX E: Uncertainty and Repeatability 59

APPENDIX F: Tip Gap Study.....62

APPENDIX G: Free Tip Turbine Picture 67

BIOGRAPHY OF THE AUTHOR.....68

LIST OF TABLES

Table 2.1 Axial flow turbine design parameters. 5

Table E.1 Uncertainty Equations 61

Table F.1 Tip Gap Case Definitions 64

LIST OF FIGURES

Figure 2.1 Non-dimensional geometry of the free tip and ducted turbine plotted against the non dimensional local radius divided by the full turbine radius. 6

Figure 2.2 The OpenProp output of the free tip turbine plotted in MATLAB [9].....7

Figure 2.3 The ducted turbine geometry from OpenProp demonstrates the graphics plotted in MATLAB [9]. 8

Figure 2.4 NACA 4412 in XFoil 9

Figure 2.5 A SolidWorks [16] model of the ducted turbine created from the OpenProp output text file. 10

Figure 3.1 A dimensioned schematic of the UMaine tow tank with the axial flow turbine in place. 11

Figure 3.2 UMaine tow tank with ducted turbine installed ready for testing. 12

Figure 3.3 An isometric view of the ducted turbine on the axial flow test platform showing the major components of the test platform.....14

Figure 3.4 A schematic drawing of the axial flow test platform viewed from one end. 15

Figure 3.5 Schematic drawing showing the end and profile views of the axial flow turbine. 17

Figure 3.6 Details AA and BB show a blown up view of the schematic in Figure 3.5. 18

Figure 3.7 Calibration graph of load cell for measuring torque vs. load cell output. 20

Figure 3.8 Torque friction as a function of turbine frequency. 21

Figure 4.1 This figure shows a single sided Fourier transform of Q during hammer test. 25

Figure 4.2 This figure shows the torque vs. samples before and after applying 30 Hz low-pass Butterworth filter. 25

Figure 4.3 A typical set of data for Q vs. samples is shown before and after filtering. 26

Figure 5.1 The free tip power coefficient vs. tip speed ratio is shown for the range of velocities and Reynolds numbers tested. 28

Figure 5.2 The free tip thrust coefficient vs. tip speed ratio is shown for the range of velocities and Reynolds numbers tested. 29

Figure 5.3 The ducted power coefficient vs. tip speed ratio is shown for the range of velocities and Reynolds numbers tested. 30

Figure 5.4 The thrust coefficient vs. tip speed ratio of the ducted turbine is shown for the range of velocities and Reynolds numbers tested. 31

Figure 5.5 The duct thrust coefficient vs. tip speed ratio is shown for the range of velocities and Reynolds numbers tested. 31

Figure 5.6 C_P vs. tip speed ratio for the ducted turbine rotor without the duct is shown with results of the same rotor with the duct. 32

Figure 5.7 C_T vs. tip speed ratio for the ducted turbine without the duct is shown with results of the same rotor without the duct. 33

Figure 6.1 Free tip average C_P vs. tip speed ratio is shown for the two carriage speeds. 34

Figure 6.2 Ducted average C_P vs. tip speed ratio is shown for the two carriage speeds.....35

Figure 6.3 Duct thrust coefficient vs. tip speed ratio is shown for the two carriage speeds. $C_D = .02$ are also shown.....39

Figure 6.4 C_L & C_D for the duct as a function of Re.....40

Figure 6.5 This figure shows the upper half of a duct with the relevant force vectors drawn in.....41

Figure 6.6 Ducted power coefficient vs. tip speed ratio of experimental data and OpenProp predictions.. 42

Figure 6.7 Free tip average C_T vs. tip speed ratio is shown for the two carriage speeds.....43

Figure 6.8 Ducted average C_T vs. tip speed ratio is shown for the two carriage speeds.....44

Figure E.1 Shows the uncertainty in C_P for the free tip and ducted turbines. 59

Figure E.2 Shows the uncertainty in C_T for the free tip and ducted turbines. 60

Figure F.1 Measuring tip gap on ducted turbine.....63

Figure F.2 C_P as a function of t/D (V = 1.25 m/s) 64

Figure F.3 Percent difference in C_P 65

Figure G.1 Picture of the free tip turbine. 67

NOMENCLATURE

c/D	chord length to rotor diameter ratio
c	chord length
c_D	cord length of duct
C_d	drag coefficient
C_L	lift coefficient of rotor
C_{LD}	lift coefficient of duct
D	diameter
Q	torque
T_D	duct thrust
T_R	rotor thrust
V	inflow velocity
Q	torque
r	local radius
R	radius of rotor
α	angle of attack of rotor
α_D	angle of attack of duct
β_i	inflow angle as seen by rotor
β_{iD}	inflow angle as seen by duct

PERFORMANCE EQUATIONS

$$C_P = \frac{Q\omega}{\frac{1}{2}\rho V^3 \pi R^2}$$ power coefficient

$$C_T = \frac{T_r}{\frac{1}{2}\rho V^2 \pi R^2}$$ thrust coefficient for rotor (no duct)

$$C_{TD} = \frac{T_D}{\frac{1}{2}\rho V^2 \pi R^2}$$ thrust coefficient of duct

$$\lambda = \frac{R\omega}{V}$$ tip speed ratio

CHAPTER 1. INTRODUCTION

As we use more and more of earth's petroleum reserves and learn about the effects of global warming, it has become critical that we find alternative energy sources to meet our electricity needs. However, no single source is likely to meet the growing global demand. The benefits and drawbacks of nuclear, solar, wind, hydro and tidal energy must all be carefully weighed, and assessments made based on thorough, research.

1.1 MOTIVATION

While in all likelihood moving water has been a power source since humans invented machines, relatively little research has been performed on axial flow tidal turbines and even less on ducted axial flow turbines. As of the date of this writing there is only one deployed, grid connected, commercial-scale tidal turbine in the world [1] . One of the most important characteristics of a turbine is the overall efficiency, which is usually reported as a coefficient of performance (C_p), or the percentage of total kinetic power that can be removed from the flow. Free tip axial flow turbines are capable of $C_p \approx .46$ [2]. In theory, ducted axial flow turbines have the potential to exceed the Betz limit of $C_p \approx .59$ [3] making them the most efficient style of hydrokinetic turbine for use in free stream flows. However, to date these efficiency claims have not been tested except with theoretical models. The key objective of this thesis is to provide a data set to be used as a part of a validated design code for ducted and unducted axial flow turbines. The actual optimization of the turbine and evaluation of efficiency claims is well beyond the scope of this thesis.

1.2 BACKGROUND

The key objective of this thesis is to provide data to be used as a part of a validated design code for ducted and unducted axial flow turbines. A substantial amount of setup and infrastructure was required to meet this end goal. Many parts of that infrastructure were in place at the University of Maine from ongoing testing of cross-flow tidal turbines [4]. A decision was made early on in this thesis to design and build as much of the experimental system around the existing faculties as possible without compromising the quality of results. This decision reduced overhead costs, setup time and expanding the knowledge base of our current systems. The major components of the infrastructure in place included:

- Tow tank
- Data acquisition system programmed in LABVIEW [5]
- Turbine motor controller setup for a Parker servo motor

This left the turbine test rig, the turbines themselves and the duct to be designed, fabricated and tested.

For several reasons a decision was also made to start testing with the free tip turbine case, which has some experimental data for marine applications but has not been exhaustively tested. The most directly applicable experiments were performed at MIT [6][7] using a 2 blade turbine designed in OpenProp and demonstrate reasonable agreement between experimental data and OpenProp predictions but further validation was desirable. The other purpose, and perhaps the dominant one for starting with the free tip turbine, was to gain benchmark data with the test rig built at the University of Maine. This benchmark data could be compared to previous work from other experiments to see

if our test rig yielded similar results. Our free tip data could then be compared to the ducted case to see if a performance increase was realized.

OpenProp was selected as the basic design tool since it is computationally efficient. The program can be run on a basic laptop computer in a matter of minutes and thus is suitable for the optimization necessary in developing an efficient turbine.

1.2.1 OpenProp

OpenProp is an open source propeller and turbine design code [8]. The design code is written in MATLAB [9] and utilizes lifting line theory and a prescribed helical wake to model the blades. A system of ring vortices and an image model are used for the hub and duct. The code was initially developed to design free tip marine propellers and then extended to include the design of ducted propellers [10] [8]. The code was later modified and has been at least partially validated for modeling of turbines. Essentially no data exists for the ducted turbine case.

For the case of the free tip propeller OpenProp was validated with experimental data and is in good agreement [6]. The ducted propeller model has been validated with the MIT Propeller Lifting Line program and is in good agreement [11] but has not been validated with experimental data. The free tip turbine case has been validated with experimental data as well and is in reasonable agreement but not as well as the propeller [6]. The ducted turbine portion of the code is still under development in OpenProp and has not been validated.

1.2.2 Free Tip Turbines

Free tip (unducted) axial flow turbines are primarily used in the wind industry for commercial applications. The designs are well developed with extensive experimental data and multiple numerical codes to optimize their design and evaluate performance.

Marine turbines are not as well developed, however several companies are working on developing codes for this purpose. There are a couple of test deployments, perhaps the most notable by Marine Current Turbines [12] owned by Siemens [13]. Currently, Marine Current Turbines has the only grid-tied commercial scale turbine in the world [1].

1.2.3 Ducted Turbines

Ducted propellers are widely applied in marine propulsion for a variety of reasons, one of which is improved efficiency [14]. Ducts are typically employed when high thrust at a relatively low ship speed (less than 5 m/s) is required [14]. Tugboats are a good example of this. Typically, marine current turbines operate under a similar operating condition, relatively low current velocity. It is therefore reasonable to investigate whether or not adding a duct to an axial flow turbine increases its efficiency as well.

1.3 THESIS OVERVIEW

The purpose of this thesis is to provide experimental data which can be used for validation of ducted and unducted axial flow tidal turbine models. The basic infrastructure used was in place from ongoing testing of cross-flow tidal turbines [4]. To the extent possible the existing experimental faculties were used. For this work the mechanical portions of the turbine test rig, the turbines and the duct had to be designing and built. The contribution of this work is to highlight the challenges of proper duct design and to provide an unducted data set for future optimization studies.

CHAPTER 2. TURBINE DESIGN AND FABRICATON

The basic parameters for the turbine design were determined largely by the capabilities of our testing apparatus. The turbine needed to provide enough torque and thrust to facilitate measurement but sufficiently small to fit in the tank. The tank dimensions are limited by both blockage and free surface effects. The design parameters for both the free tip and ducted turbines and can be seen in Table 2.1.

Table 2.1 Axial flow turbine design parameters.

Parameter	Symbol	Value	Units
Turbine Diameter	D	.254	m
Carriage speed	V	1.25	m/s
Lift Coefficient (Blades)	C_L	.5	
Lift Coefficient (Duct)	C_{LD}	.5	
Drag Coefficient	C_d	.02	

It is important to note that the free tip and ducted turbines do not have the same geometry; they are both optimized by OpenProp for their respective case. The objective of this thesis is not to compare a free tip turbine to a ducted turbine but rather to obtain experimental data from a ducted turbine. The free tip turbine is however a useful way of checking the design and testing methods. To illustrate the differences of the two blades Figure 2.1 shows both the free tip and ducted turbine geometry. Table of the non-dimensional geometry can also be seen in Appendices B and D.

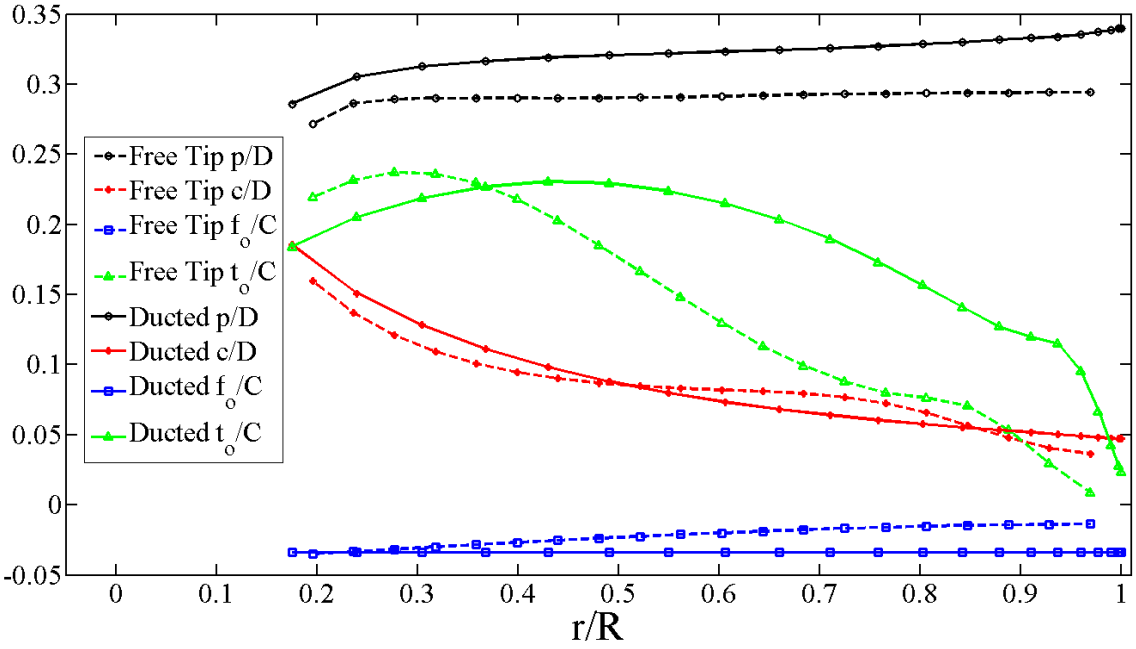

Figure 2.1 Non-dimensional geometry of the free tip and ducted turbine plotted against the non dimensional local radius divided by the full turbine radius.

2.1 FREE TIP TURBINE DESIGN

The free tip turbine was designed using OpenProp. No code modifications were required for the unducted turbine case. The code was run directly using a MATLAB [9] script, not the OpenProp GUI. Use of the GUI limits the number of parameters that can be modified. Plots from OpenProp were also customized which is not possible with the GUI. An example of the output is the turbine geometry shown in Figure 2.2. The input for OpenProp can be seen in Appendix A.

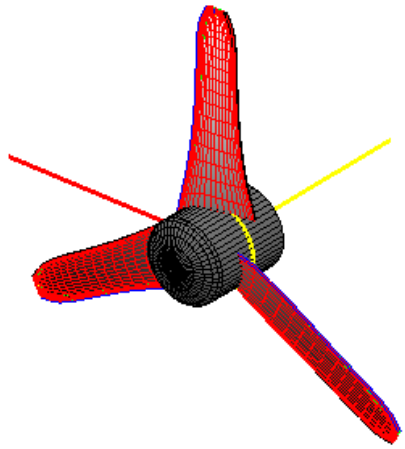

Figure 2.2 The OpenProp output of the free tip turbine plotted in MATLAB [9].

2.2 DUCTED TURBINE DESIGN

The rotor for the ducted turbine was also designed using OpenProp, but the duct was only partially designed with this code. OpenProp optimizes the blades for the ducted turbine but does not optimize the duct. The code calculates the circulation of the blades and the duct, finds the influence of the duct and the blades on each other and then iterates until the blade circulation converges [11][8]. The code also calculates the lift coefficient of the duct (C_{LD}) required to obtain the correct duct circulation as well as the inflow angle for the duct (β_{iD}). The duct thrust coefficient (C_{TD}), and the duct chord length (C_D), are entered as inputs. The rotor was placed at the ¼ chord of the duct (from leading edge). This location was chosen by moving the location of the rotor along the duct chord in OpenProp and selecting the location that corresponded with the highest C_p. Figure 2.3 shows MATLAB [9] graphic of the ducted turbine. The input code for OpenProp can be seen in Appendix C.

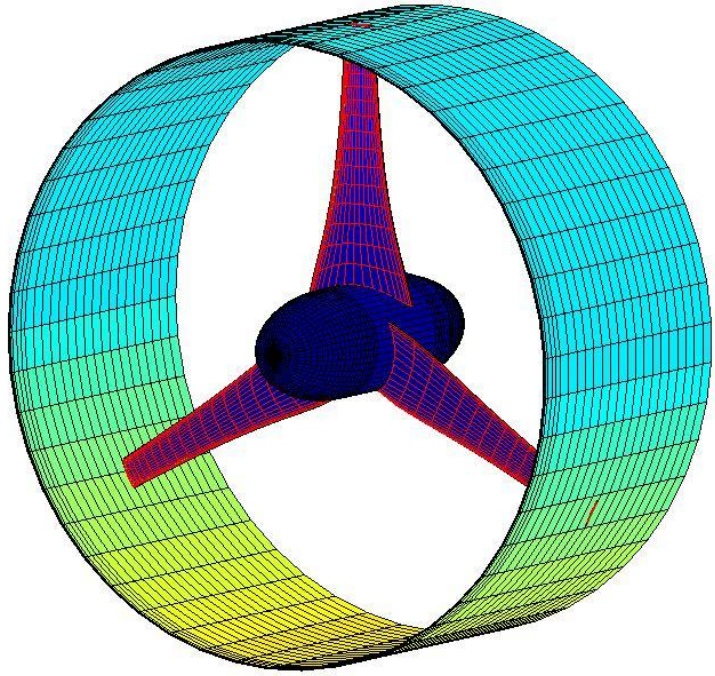

Figure 2.3 The ducted turbine geometry from OpenProp demonstrates the graphics plotted in MATLAB [9].

2.2.1 Duct Geometry

Since the duct geometry is not modeled in OpenProp it must be designed separately. OpenProp outputs basic parameters for the duct, specifically the inflow angle as seen by the duct (β_{iD}) and the required lift coefficient of the duct (C_{LD}). Based on these values and the duct cord length (C_D) a duct profile and angle of attack can be determined. A duct foil profile that supplies the correct C_{LD} is then selected. For the current case OpenProp provide, $C_{LD} = .5$, $\beta_{iD} = -1^{\circ}$ and $C_d = .127m$. A NACA 4412 was selected as the profile and XFoil [15] was used to obtain the lift coefficient at a zero degree angle

of attack (Figure 2.4 NACA 4412 in XFoil). The profile was then set at $\beta_{iD} = -1^{o}$ to maintain a zero degree attack angle as specified in XFoil.

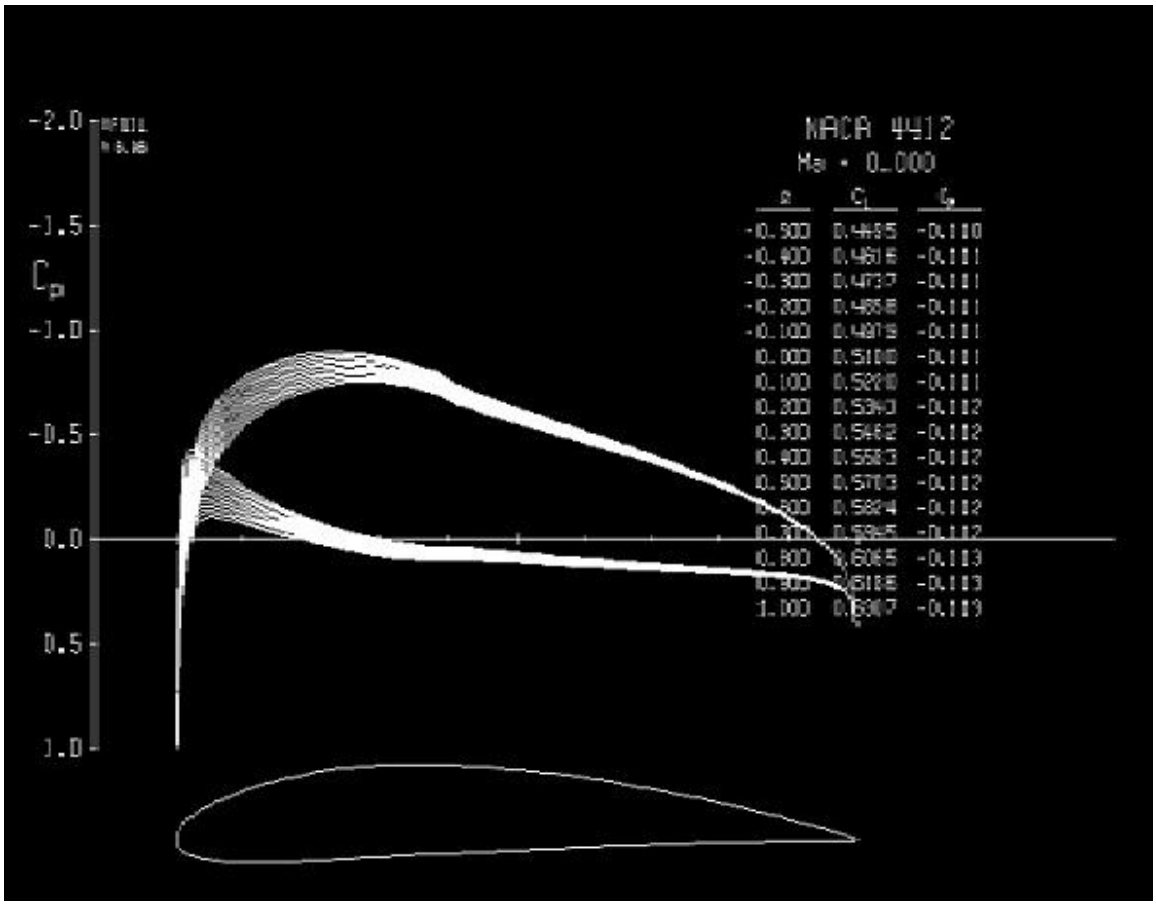

Figure 2.4 NACA 4412 in XFoil

2.3 TURBINE FABRICATION

Several methods of producing the turbine blades were considered; 3D printing was selected for these turbine blades. OpenProp outputs a text file of 3D points for the blade geometry, which can be imported into SolidWorks [16] to create a part. The duct was also modeled in SolidWorks [16] using the profile of a NACA 4412. The ducted turbine model can be seen in Figure 2.5.

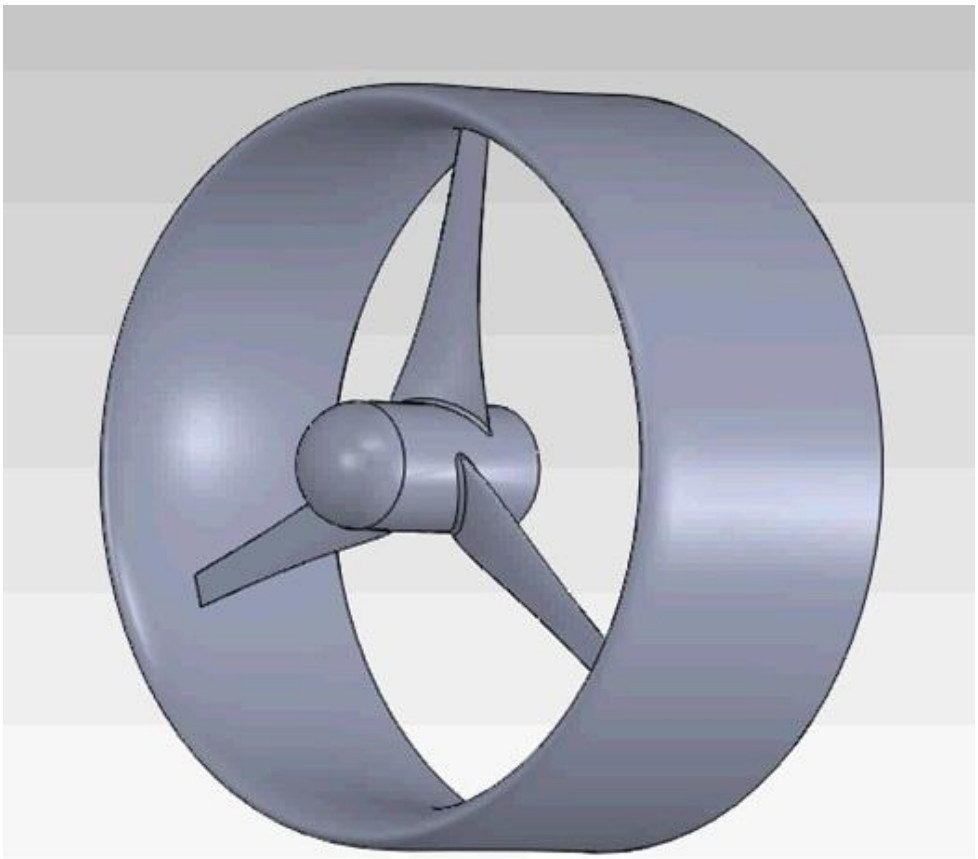

Figure 2.5 A SolidWorks [16] model of the ducted turbine created from the OpenProp output text file.

CHAPTER 3. EXPERIMENTAL TESTING

3.1 EXPERIMENTAL SETUP

This chapter describes the infrastructure and procedures used for collecting data. The tow tank, motor controller and data acquisition were in place from previous testing performed for a cross-flow turbine [4].

3.1.1 Tow Tank

UMaine's tow tank was utilized for all data collection. The tank is 2.44 meters wide, 1 meter deep and 30 meters long, and is capable of carriage speeds up to 1.5 meters per second. The carriage is mounted on sided rails and driven by an endless wire rope wrapped around a drive drum [4]. Figure 3.1 shows the dimensions of the tow tank and the position of the axial flow turbine. Figure 3.2 shows the tow tank with the ducted turbine during testing.

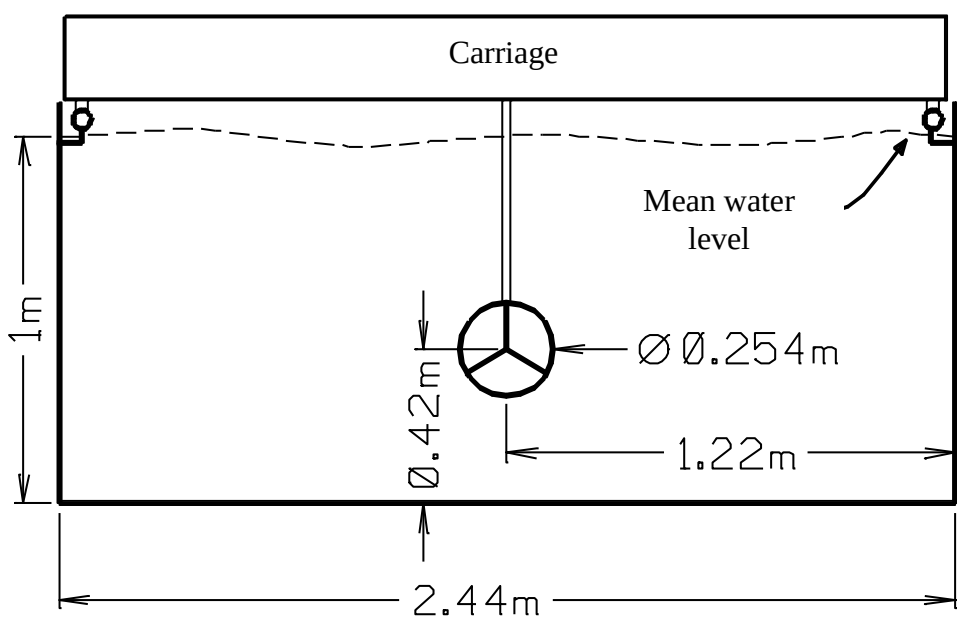

Figure 3.1 A dimensioned schematic of the UMaine tow tank with the axial flow turbine in place.

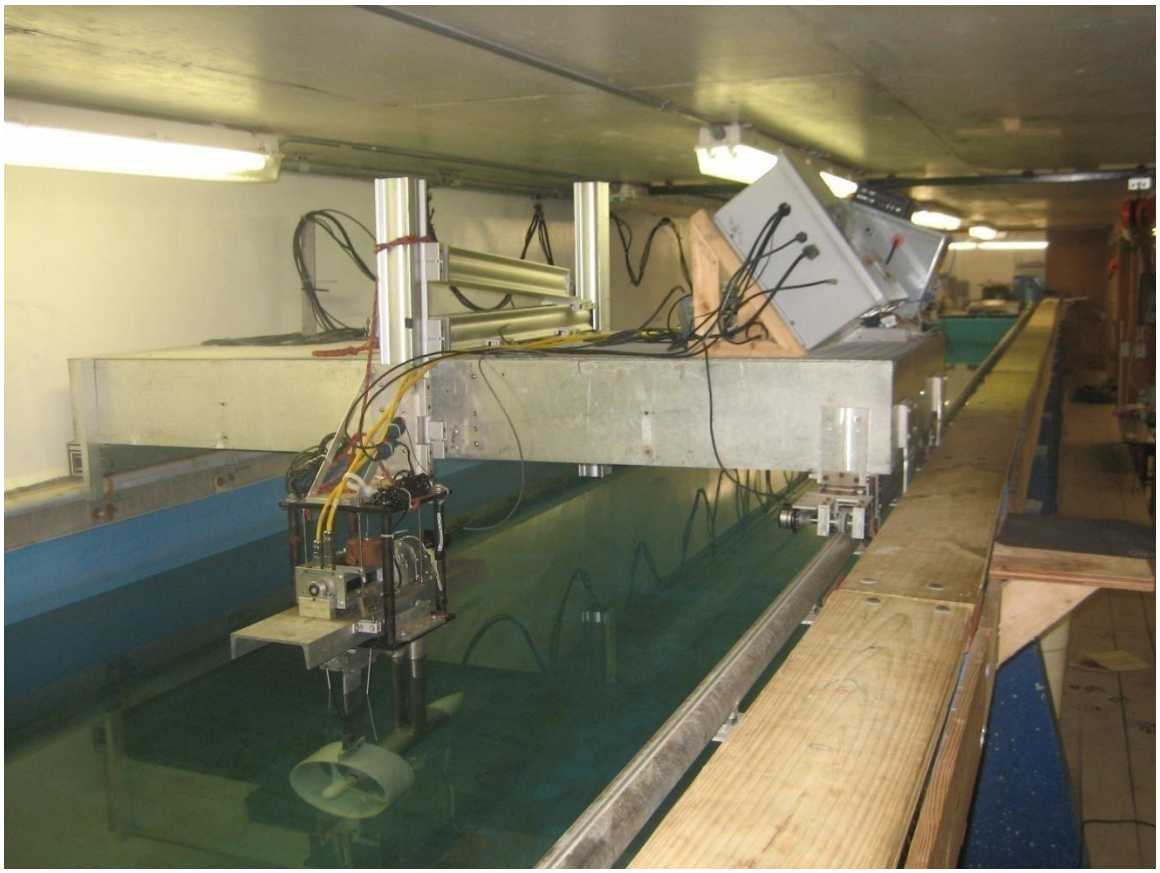

Figure 3.2 UMaine tow tank with ducted turbine installed ready for testing.

3.1.2 Axial Flow Turbine Test Platform

The turbine test platform was fabricated at UMaine. The turbine testing system consists of a wet hub and shaft connected via a chain to an above-water shaft. The chain drive is a one-to-one ratio with the chain running in water for most of its length. The dry upper shaft is connected to a Parker [17] servo motor to regulate turbine frequency. The servo motor controller is configured to either drive the turbine or absorb energy. This flexibility eliminates self starting issues and allows the turbine to be operated at negative power coefficients if required.

The entire motor drivetrain is suspended on slender rods attached to a mounting frame. This allows a small amount of motion in the horizontal direction unrestrained by friction. A load cell is in place to prevent the horizontal motion and to record thrust from the underwater body. Schematic drawings illustrating this may be seen in Figure 3.4 Figure 3.5 and Figure 3.6. The other two load cells shown in Figure 3.5 and Figure 3.6 are for measuring torque and duct thrust. They are explained in the following section.

Data is collected in real time using LABVIEW [5] and a National Instruments CRIO [5] data acquisition system. The test platform was designed to be compatible with the existing data collection and control systems in place [4]. Figure 3.3 shows the axial flow test platform with major components labeled.

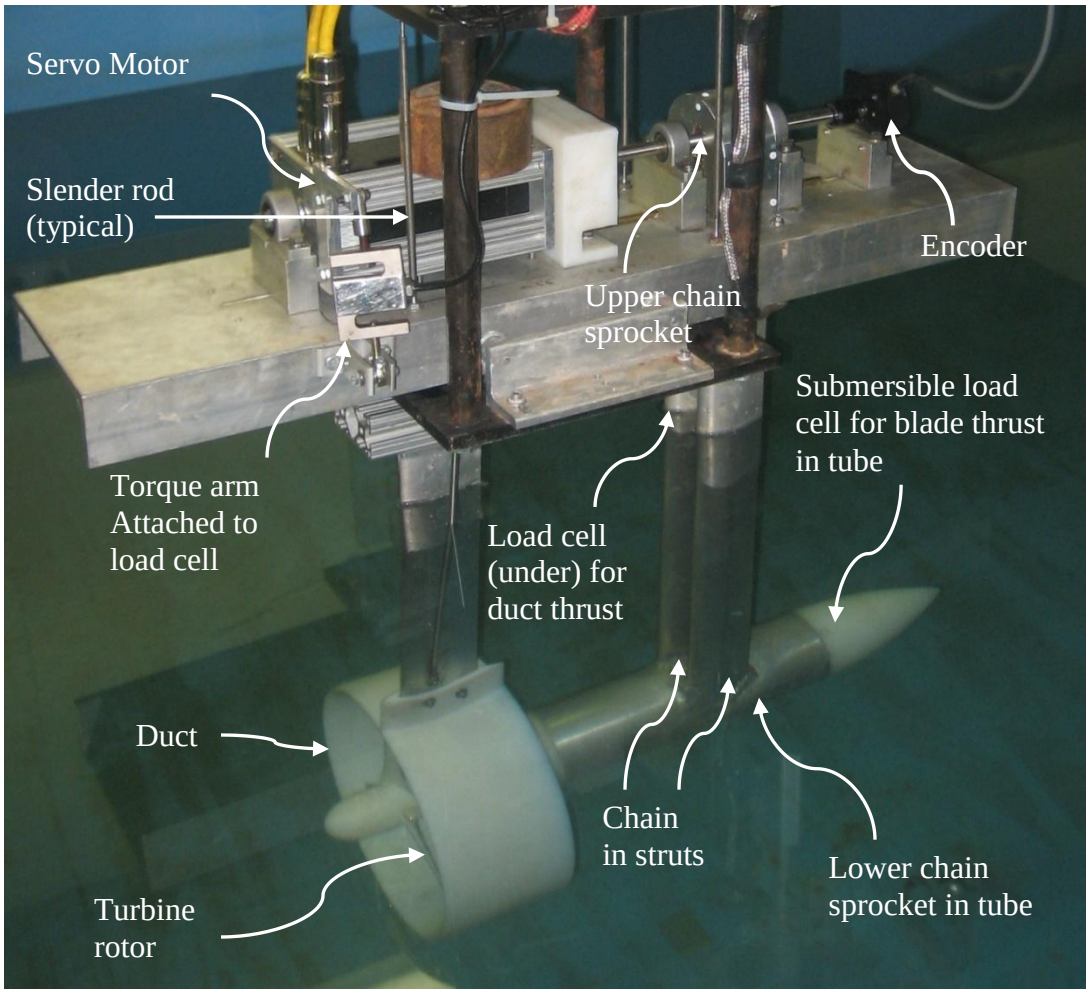

Figure 3.3 An isometric view of the ducted turbine on the axial flow test platform showing the major components of the test platform.

3.1.3 Measured Quantities

Controlled parameters were measured to track variations in desired settings. Additional measurements were also taken to perform a full range of performance characterization. All measured quantities were recorded at a sample rate of 1 kHz. The measured quantities were recorded simultaneously to allow for correlation at each time step. Data acquisition starts after the acceleration period of the tow tank carriage and the data acquisition is stopped before the ramp-down or deceleration period to simplify post

processing. This is consistent with normal tow tank practice and the signal procession discussed in Chapter 4 applies only to the time period when the carriage is at the test speed. Time is recorded in the data acquisition system using a 266 MHz clock speed [4].

3.1.3.1 Torque

Torque is used in calculating the power coefficient (C_p). Torque data is acquired from an S-type load cell mounted on a lever arm at a known distance from the upper shaft's center of rotation. Figure 3.4 shows the orientation of the load cell and motor on the axial flow test bed.

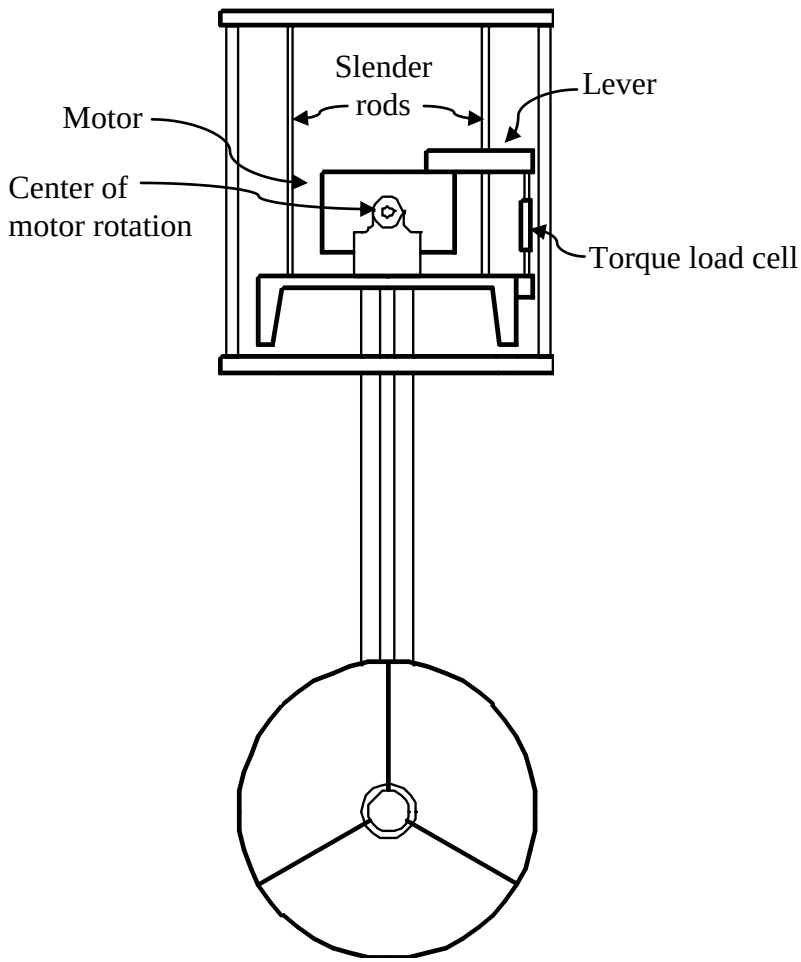

Figure 3.4 A schematic drawing of the axial flow test platform viewed from one end. The load cell to measure torque is shown.

3.1.3.2 Rotor Thrust

Rotor thrust is used in calculating the thrust coefficient (C_T). Rotor thrust is measured using a submersible S-type load cell mounted in the downstream side of test platform hub. The lower shaft pushes on the load cell via a thrust bearing. Figure 3.5 and Figure 3.6 illustrate the load cell and shaft.

3.1.3.3 Duct Thrust

Duct thrust is used in calculating the duct thrust coefficient (C_{TD}). Duct thrust is measured from an S-type load cell. The load cell measures lateral force on the entire underwater apparatus. This includes drag from the support struts, blade thrust and turbine thrust. The blade thrust and drag are then subtracted during post processing from the overall thrust to obtain the duct thrust. Figure 3.5 and Figure 3.6 illustrate the load cell that measures duct thrust.

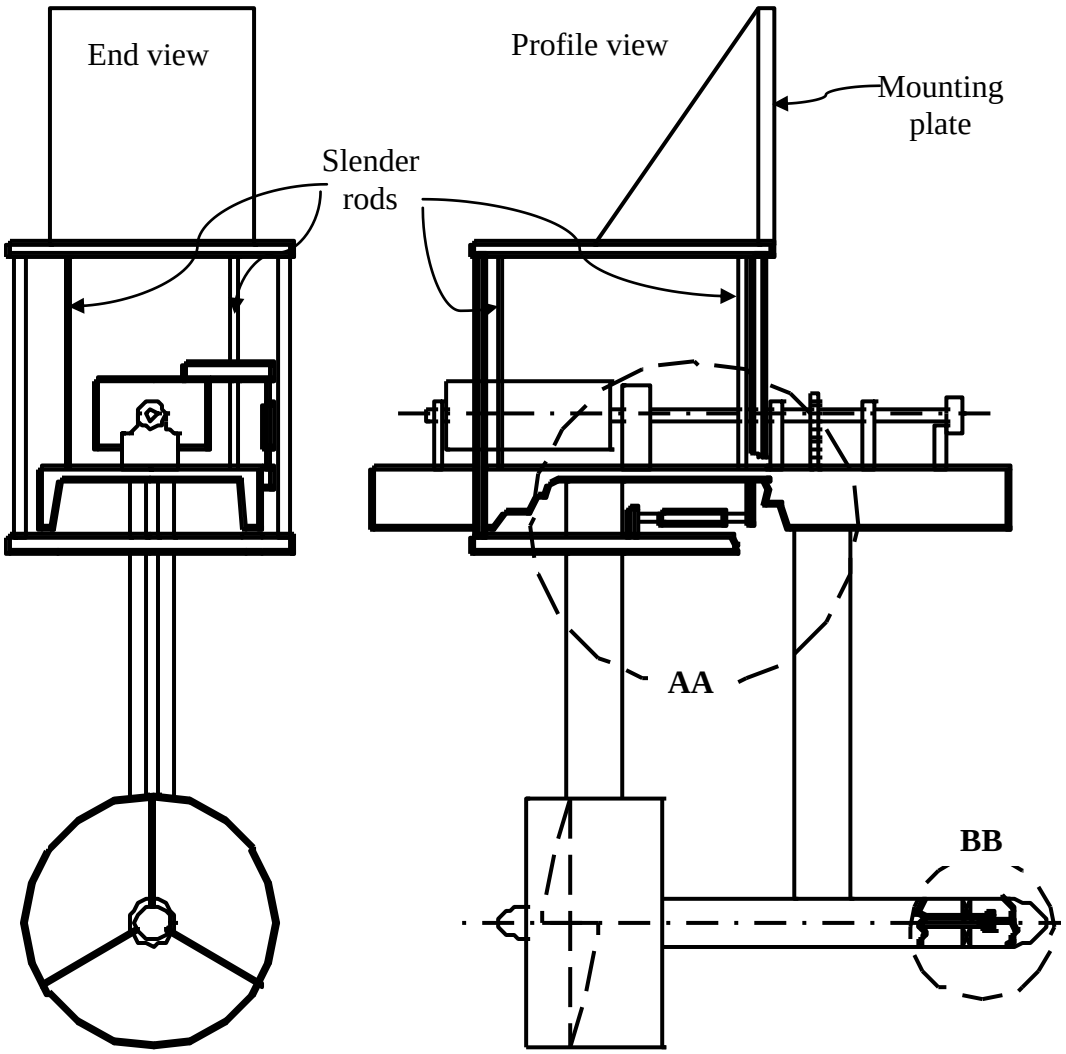

Figure 3.5 Schematic drawing showing the end and profile views of the axial flow turbine. Also shown are the load cells for the duct thrust and blade thrust.

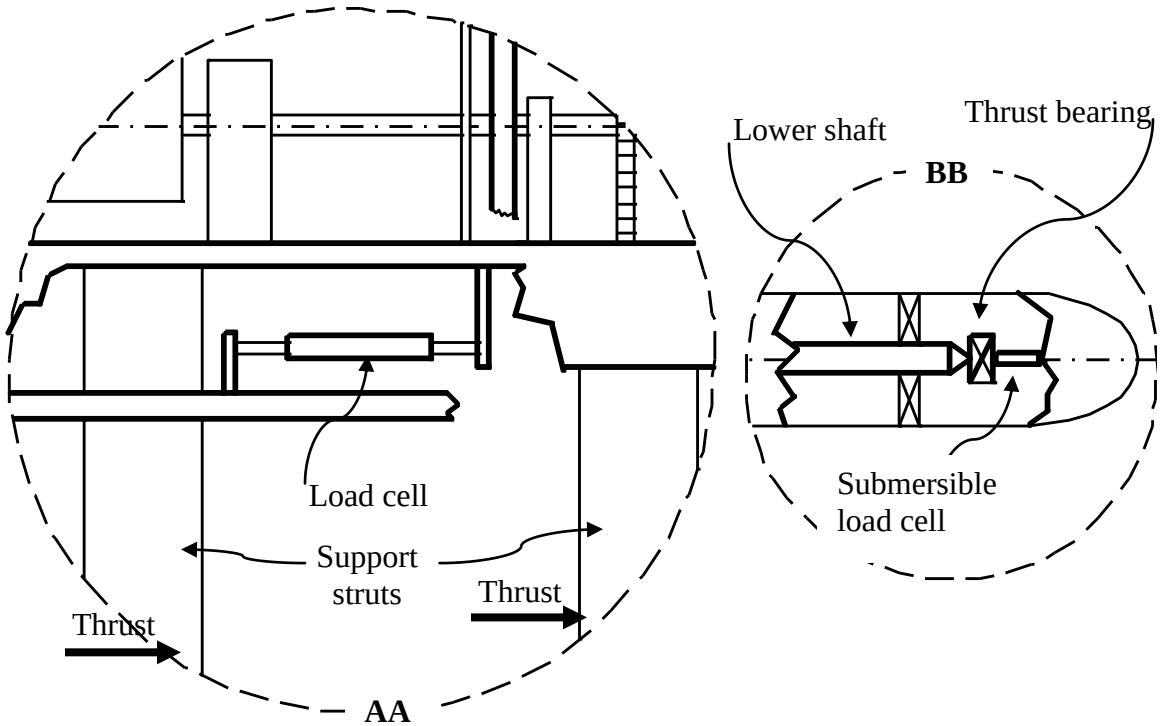

Figure 3.6 Details AA and BB show a blown up view of the schematic in Figure 3.5. AA shows the load cell used for measuring duct thrust. BB shows the load cell used for blade thrust.

3.1.3.4 Turbine Frequency

Turbine frequency (ω) is used in calculating the tip speed ratio(λ). The drivetrain utilizes a position encoder to calculate the turbine frequency from the derivative of the position with respect to time [4].

3.1.3.5 Inflow Velocity

Inflow velocity (V) is also used in calculating the tip speed ratio (λ). The inflow velocity is measured with a position encoder mounted on the tow tank carriage. A rubber wheel rides on the carriage and drives the encoder. The velocity is obtained by taking the derivative of the position with respect to time [4].

3.2 TEST METHODS

Consistent methodical tests were required to obtain usable data from these experiments. This section explains the calibrations and testing methods performed for this thesis.

3.2.1 Calibration

Calibrating the load cells and accounting for friction losses were the most difficult and essential steps for this thesis. Friction losses, especially for torque, are significant and without properly accounting for it, the resulting data is of little value.

3.2.1.1 Torque Calibration

Torque calibration is crucial to obtained meaningful power coefficient results. A calibration of the torque was performed by placing weights on a lever arm attached to the motor. The motor is free to rotate on its bearings, and the force on the torque load cell was recorded. Three trials were performed, each trial consisting of five incrementally heavier weights. The average of the data from each trial was used to obtain an equation for the torque (Q). The data points and curve fit can be seen in Figure 3.7.

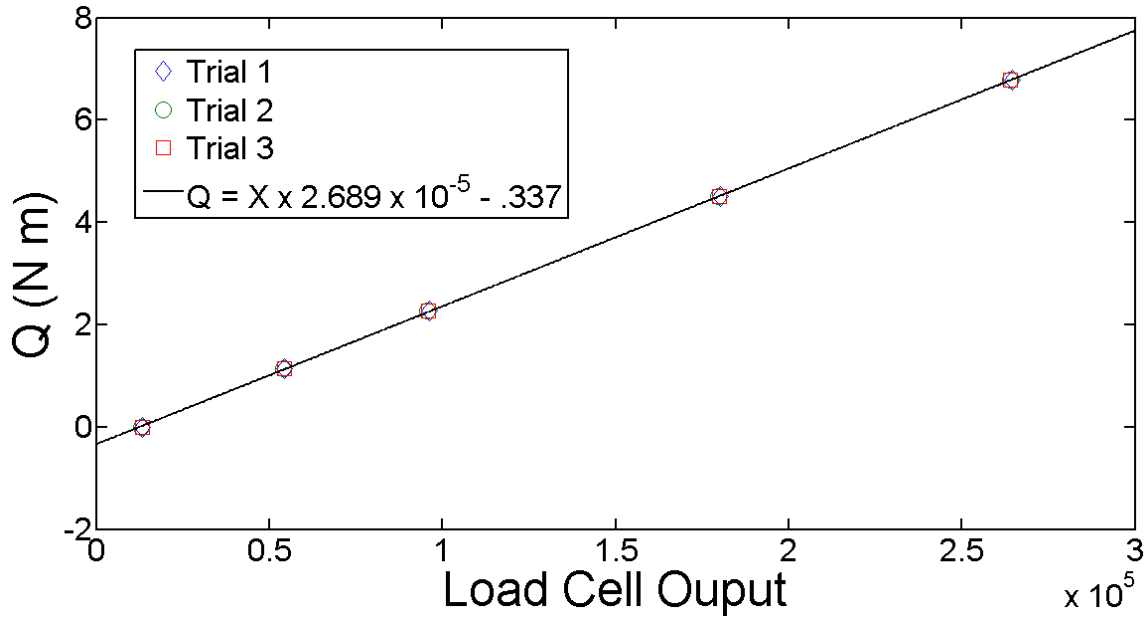

Figure 3.7 Calibration graph of load cell for measuring torque vs. load cell output.

The friction in the drivetrain was measured as a function of turbine frequency. Water acted as a lubricant to the turbine making friction losses in the system significantly lower when the turbine was in the water compared to out of the water. Therefore, friction losses from the drivetrain were measured "wet". By placing the test platform in the tank without a rotor and creating a torque curve (which is important to create a C_P curve) only the parasitic losses were measured. A third order polynomial ($Q = -5.01 \times 10^{-8}\omega^3 + 1.44 \times 10^{-5}\omega^2 + 1.33 \times 10^{-4}\omega + Q_o\ Nm$) fit to the data gave the frictional loss in torque as a function of turbine frequency where Q_o is the offset and ω is in rad/s. Figure 3.8 shows the calculated curve along with two sets of experimental data.

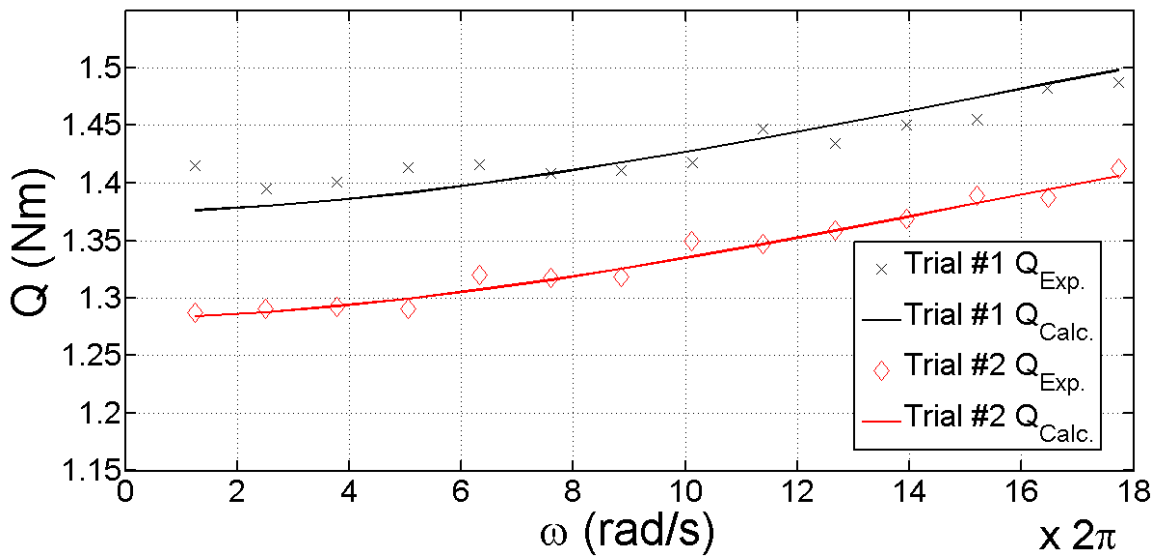

Figure 3.8 Torque friction as a function of turbine frequency. Two sets of data are shown plotted with the calculated curve using two different offsets.

The offset term in Q_o was measured often during testing to ensure any irregularities in rotational friction were accounted for. Due to the difficulty of removing the turbine from the test platform during testing the torque offset was measured by operating the test platform with the turbine in place at a very slow rotational speed. The low turbine speed was not sufficient to create any lift in the turbine blades to contribute to the torque. The torque offset term was measured at least three times (sometimes more) for every C_p curve, at the beginning, middle and end of each data set. The average of these three values was used as the offset term Q_o. Figure 3.8 shows a typical variation in offset before correction.

3.2.1.2 Rotor Thrust Calibration

A calibration equation for the rotor thrust (T_R) load cell was determined in a similar fashion to the equation for the torque load cell. Incrementally heavier, known weights

were applied to the load cell and the output recorded. A polynomial was then fitted to the experimental data. The offset for the polynomial was established by performing a tow tank run with the free tip turbine in place at a low carriage speed ($0.0762\ m/s$). The force on the load cell is negligible at a low carriage speed so the offset could be established for zero force. Since the load cell for the rotor thrust is mounted in the test platform hub and pushed on directly by the rotor via the lower shaft there was no drag force to account for with this measurement. Figure 3.5 and Figure 3.6 illustrate the load cell and lower shaft.

3.2.1.3 Duct thrust Calibration

The load cell for the duct thrust (T_D) was also calibrated in a similar manner to the rotor thrust calibration. An additional complication to measuring the duct thrust was that the duct thrust load cell measured the force for the entire underwater body (T_{OA}). The sum of the rotor thrust, the duct thrust and the test platform drag (D_{OA}) created by the support struts was measured. The rotor thrust and strut drag from previous tests was subtracted to obtain the duct thrust as seen in (3.1).

$$T_D = T_{OA} - T_R - D_{OA}\ (N) \tag{3.1}$$

3.2.2 Turbine Test Procedure

A standard operating procedure was established for testing. All testing in the tow tank was performed in the same sequence each time to minimize variations in the data. Each data point shown in a performance curve (C_p, C_T etc.) was obtained from a complete carriage run at a fixed tip speed ratio. The carriage and turbine were

accelerated to the desired velocity before data recording started. A minimum of 28 turbine revolutions were obtained for each data point (typically about 15 seconds). Recording ended prior to carriage deceleration [4].

The range of tip speed ratios for a typical curve in this testing is $1 \leq \lambda \leq 10$ at $\lambda = 0.75$ increments. The turbine is operated at a very low frequency, typically 0.19 Hz, at the beginning, middle and end of testing for the range of tip speed ratios. These low frequency tests are averaged to obtain the offset in the torque load cell. The offset is applied to the measured C_p for these tip speed ratios.

Performance is expressed non-dimensionally. However, it was desirable to perform testing at different inflow velocities (V). Two inflow velocities, $V = 0.91\ m/s$ and the design velocity, $V = 1.25\ m/s$ were chosen. This was done to see what affect changing the Reynolds number would have on performance.

Blockage effects were not corrected for in the data and are not considered substantial since the ratio of tow tank area to turbine area, $\frac{A_{tank}}{A_{turbine}} = 48$. This is a much larger ratio than is generally considered significant for blockage effects to be considered [18]. Figure 3.1 shows the dimensions of the axial flow turbine and tow tank.

For the ducted turbine the tip gap ratio ($\frac{t_g}{D}$) was limited to 0.0039 or less based on a tip gap study performed for this thesis (Appendix F) and previously published data for propellers [19][20]. For this turbine $\frac{t_g}{D} = .0039$ translates to 1mm of gap between the rotor tip and duct.

CHAPTER 4. DATA PROCESSING

The data acquisition programmed in LABVIEW [5] provided a binary raw data file that was post processed in MATLAB [9]. Processing the data consisted of separating the binary file into data vectors and calculating calibrated quantities of interest. Filtering was used to remove noise. The mean value of the filtered data is used for calculating performance parameters.

4.1 FILTERING

Noise from the system consisted of mechanical electrical and other sources. Filtering of the data was accomplished in MATLAB [9] using a low-pass Butterworth filter. A hammer test was performed to determine the natural frequency of the system. The natural frequency for this system was in the 38 Hz range as seen in Figure 4.1. A range of filter cutoff levels between 18 Hz to 38 Hz was tried with virtually no change to the mean value of the performance parameters before and after filtering. 30 Hz was chosen as a good middle ground for the cutoff since it provides an adequately clean signal with no risk of over filtering; particularly as mean values were used for calculations. The filtered results of the hammer test can be seen in Figure 4.2. Figure 4.3 shows a typical set of data for Q before and after filtering along with the mean value for both the filtered and unfiltered data. The mean of Q before filtering is -1.201Nm compared to the mean after filtering of -1.200Nm.

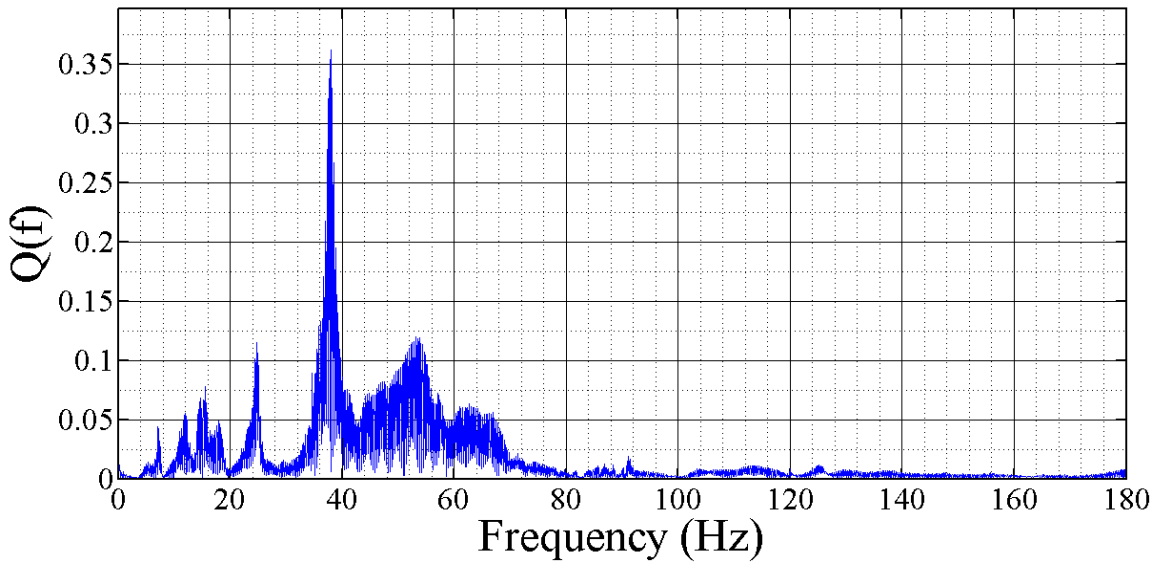

Figure 4.1 This figure shows a single sided Fourier transform of Q during hammer test.

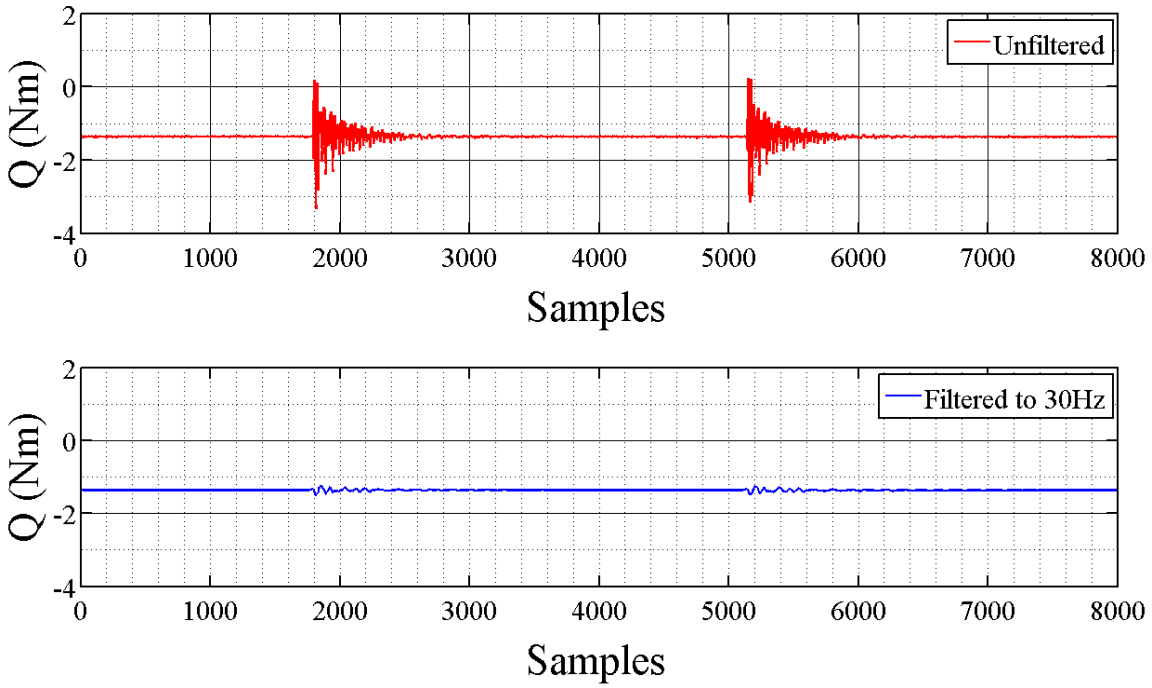

Figure 4.2 This figure shows the torque vs. samples before and after applying 30 Hz low-pass Butterworth filter.

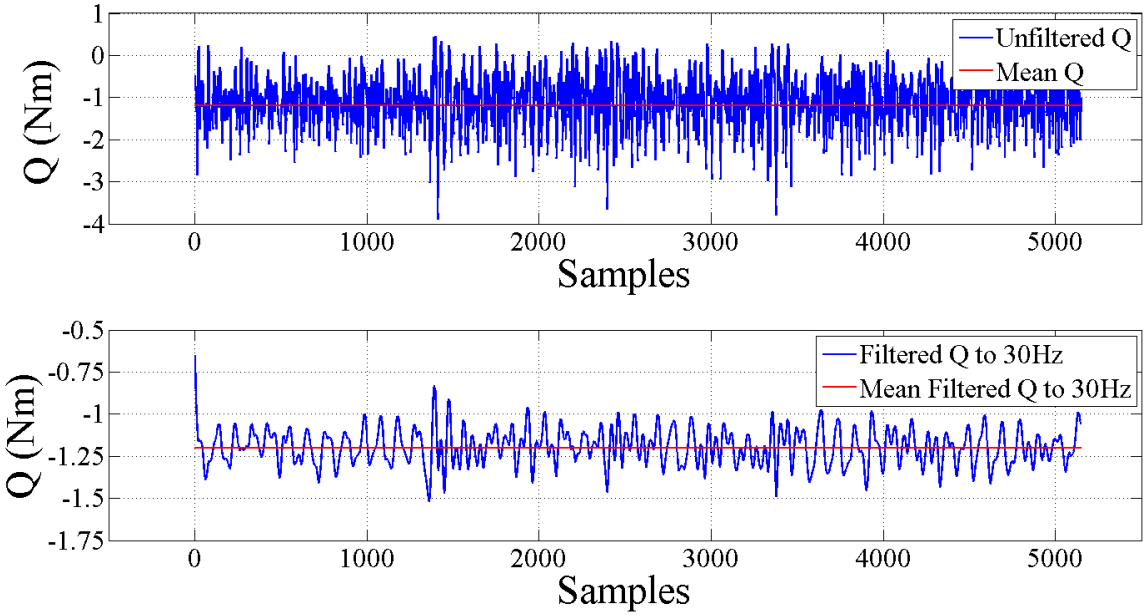

Figure 4.3 A typical set of data for Q vs. samples is shown before and after filtering. The mean values for the filtered and unfiltered data are also displayed.

Figure 4.3 shows the entire data set acquired for a single carriage run. It was not necessary to remove data from the beginning or the end of the run when the carriage is accelerating or decelerating in post processing since that data is not acquired with the data acquisition system.

CHAPTER 5. RESULTS

The results from the experimental work performed for this thesis are presented and described in this chapter. The actual data points instead of mean and range are plotted in order to provide raw data for other researchers. The most important objective of this work is to provide data for model validation. This type of validation data set with an open source turbine is currently lacking, in particular ducted turbine data is currently very limited. Further discussion of the results and conclusions are reserved for Chapter 6.

Results are grouped by estimated Reynolds number. The tests were performed at two different times of the year and consequently at two different water temperatures, the water in the tow tank changed by approximately $9.5° \, C$ over this period. This change in temperature was sufficient to have impacted the testing results. In addition, the two carriage velocities tested display different performance which is also likely to be related to the Reynolds number. Thus, it was determined to be reasonable to group the data by the approximate Reynolds number.

5.1 FREE TIP RESULTS

The free tip turbine was designed to optimize output and as such the blade chord length tapers towards the tips with increasing radius as shown in Figure 2.1. The turbine was tested at a range of tip speed ratios for four different conditions shown in Figure 5.1. The data is non-dimensionalized so would ideally lay on top of each other for all of the conditions. This is in fact the case at lower tip speed ratios. The data was taken at two different times with a difference of 9.5 degrees in water temperature increase. In

addition, between test sessions the tips of the blades were chipped during handling. The effect of this is primarily evident in the C_P data.

5.1.1 Free Tip C_P

In Figure 5.1 the coefficient of performance is shown for the free tip turbine. The maximum of the averaged C_p for $V = 0.91\ m/s$ is $C_p = 0.41$ and occurred at $\lambda = 4.45$, $Re \approx 104000$. The maximum of the averaged C_p for the designed inflow velocity, $V = 1.25\ m/s$ is $C_p = 0.44$ and occurred at $\lambda = 4.43$, $Re \approx 142000$. The data in Figure 5.1 for Re ≈ 10400 appears to be higher than expected when compared to $Re \approx 111000$. Increased blade roughness would explain this difference by causing the flow to be moved out of the transitional region thus having the same effect as increasing Reynolds number. A picture of the turbine with damaged blade tips can be seen in Appendix G.

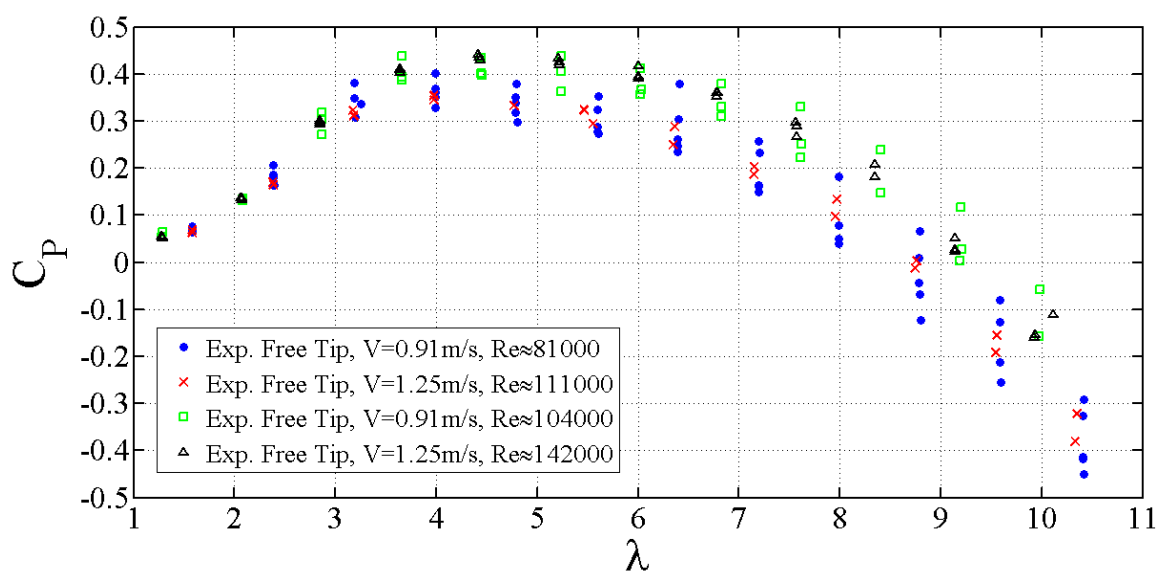

Figure 5.1 The free tip power coefficient vs. tip speed ratio is shown for the range of velocities and Reynolds numbers tested.

5.1.2 Free Tip C_t

The data in Figure 5.2 is for the thrust coefficient (C_t) results of the free tip turbine. The turbine was tested at $V = 0.91\ m/s$ and $V = 1.25\ m/s$. The maximum of the averaged C_t for $V = 0.91\ m/s$ is $C_t = 0.72$ and occurred at $\lambda = 5.24,\ Re \approx 104000$. The maximum of the averaged C_t for $V = 1.25\ m/s$ is $C_t = 0.74$ and occurred at $\lambda = 5.22,\ Re \approx 142000$.

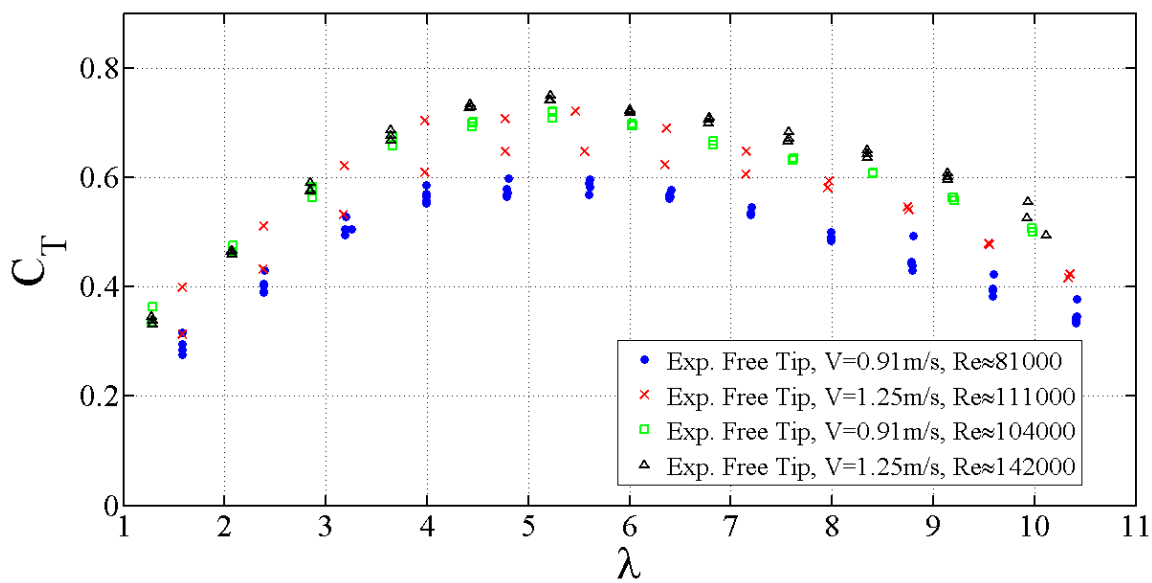

Figure 5.2 The free tip thrust coefficient vs. tip speed ratio is shown for the range of velocities and Reynolds numbers tested.

5.2 DUCTED RESULTS

The second turbine that was developed for this thesis was a ducted turbine for which the design was optimized to work with the duct. The ducted turbine chord length does not taper with increasing radius like the free tip turbine as shown in Figure 2.1. The testing for the ducted turbine was carried out for the same conditions as used for the free tip turbine. The data is also non-dimensionalized with similar Reynolds number effects due to water temperature changes as seen in the free tip turbine.

5.2.1 Ducted C_P

Figure 5.3 shows the C_p results of the free tip turbine at $V = 0.91\ m/s$ and $V = 1.25\ m/s$. The maximum of the averaged C_p for $V = 0.91\ m/s$ is $C_p = 0.36$ and occurred at $\lambda = 3.65$, $Re \approx 104000$. The maximum of the averaged C_p for the designed inflow velocity, $V = 1.25\ m/s$ is $C_p = 0.40$ and occurred at $\lambda = 4.40$, $Re \approx 142000$.

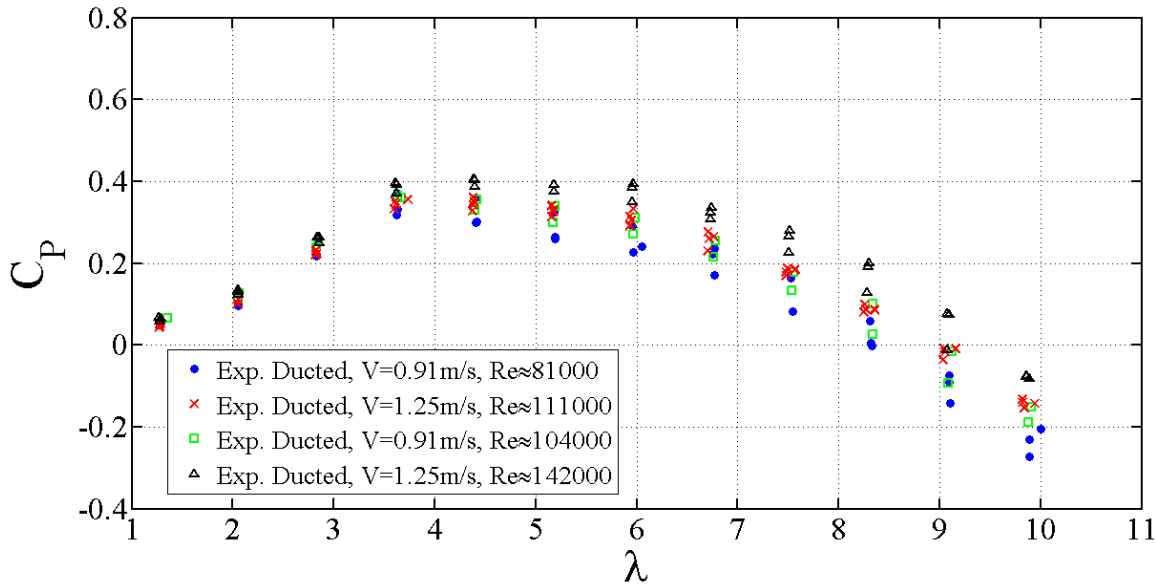

Figure 5.3 The ducted power coefficient vs. tip speed ratio is shown for the range of velocities and Reynolds numbers tested.

5.2.2 Ducted C_t

Figure 5.4 shows the C_t results of the ducted turbine at $V = 0.91\ m/s$ and $V = 1.25\ m/s$. The maximum of the averaged C_t for $V = 0.91\ m/s$ is $C_t = 0.67$ and occurred at $\lambda = 5.94$, $Re \approx 104000$. The maximum of the averaged C_t for $V = 1.25\ m/s$ is $C_t = 0.68$ and occurred at $\lambda = 5.96$, $Re \approx 142000$.

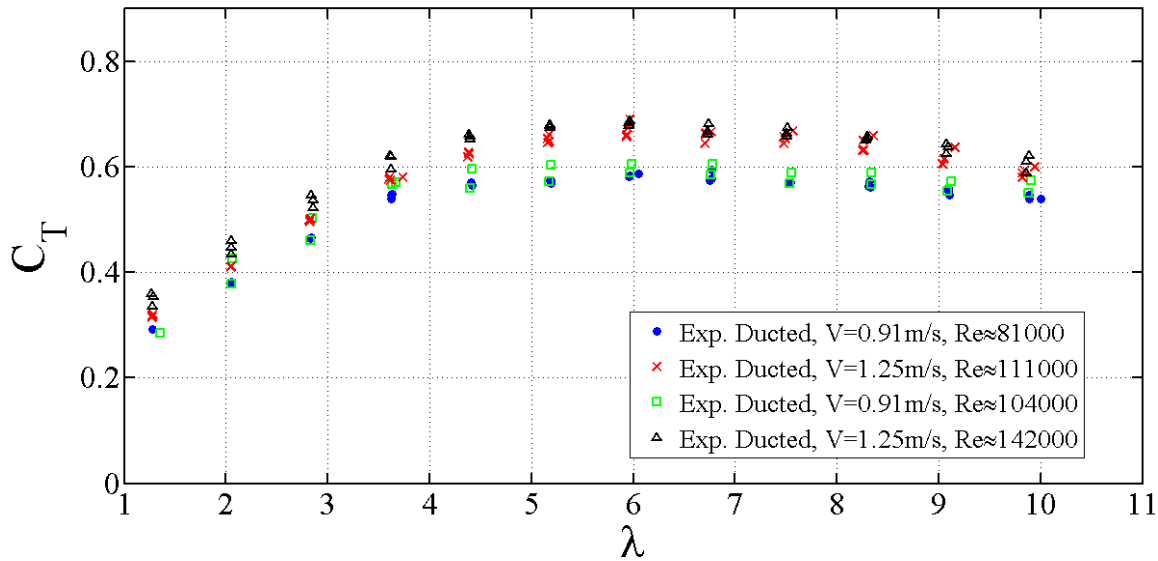

Figure 5.4 The thrust coefficient vs. tip speed ratio of the ducted turbine is shown for the range of velocities and Reynolds numbers tested.

5.2.3 Duct Thrust Coefficient

The duct thrust coefficient (C_{TD}) is shown below in Figure 5.5 Note that C_{TD} has an average of about at $C_{TD} \approx .08$ and remains almost flat through the range of λ.

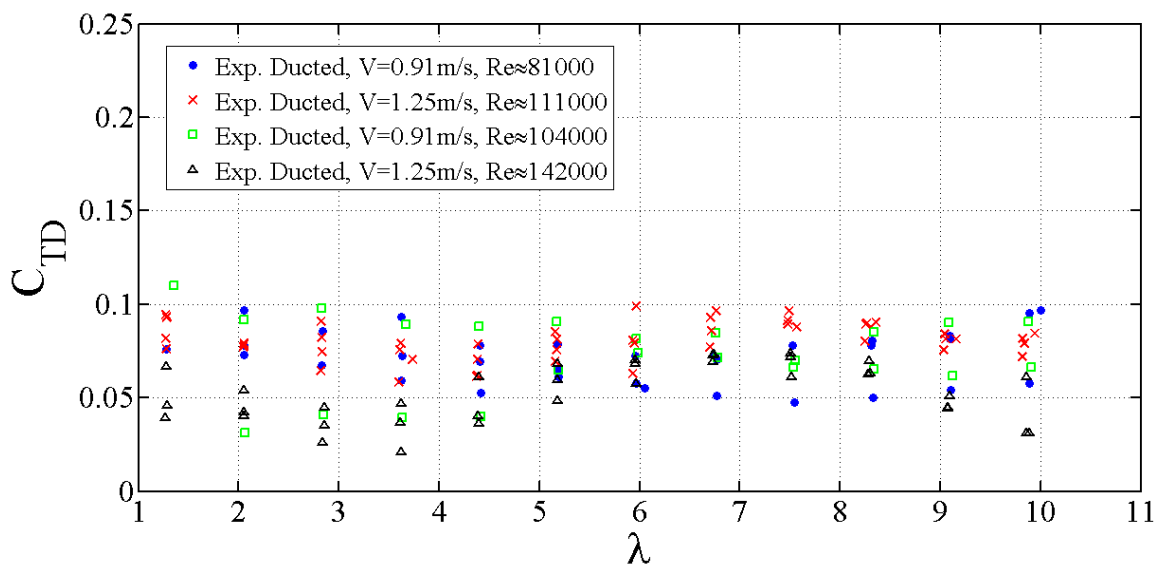

Figure 5.5 The duct thrust coefficient vs. tip speed ratio is shown for the range of velocities and Reynolds numbers tested.

5.2.4 Ducted Turbine Rotor Without Duct

Testing was performed on the ducted turbine to examine what effect the duct had on the rotor. This was accomplished by testing the rotor used for ducted turbine testing with the duct removed. While this is not the focus of this thesis it is useful in ascertaining the overall effect of the duct.

5.2.4.1 C_P For Ducted Turbine Rotor Without Duct

Figure 5.6 shows that the duct had very little effect on C_p. The results from the two Reynolds numbers tested ($Re \approx 104000$ and $Re \approx 142000$) compared to the tests with the duct in place are within the range of uncertainty defined in Appendix E and therefore statistically the same. The Reynolds number effects seen throughout the other results can also be seen here.

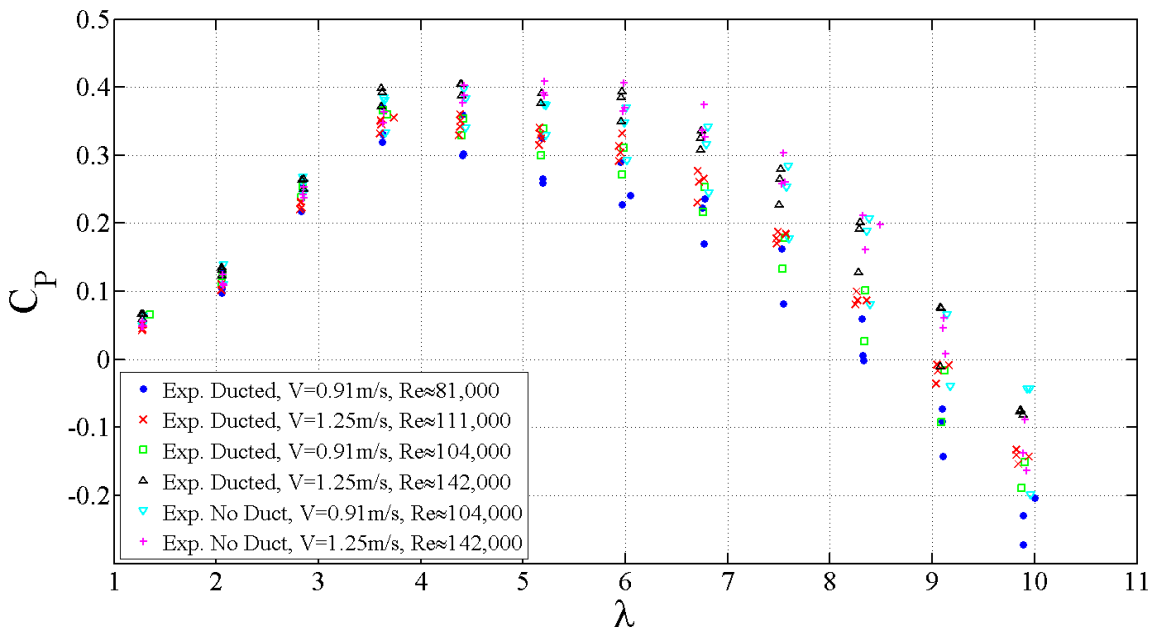

Figure 5.6 C_P vs. tip speed ratio for the ducted turbine rotor without the duct is shown with results of the same rotor with the duct.

5.2.4.2 C_t For Ducted Turbine Without Duct

Figure 5.7 show the results of the thrust coefficient for the ducted turbine without the duct plotted with the results for the ducted turbine with the duct. The thrust coefficient shows a small overall increase without the duct verses with the duct.

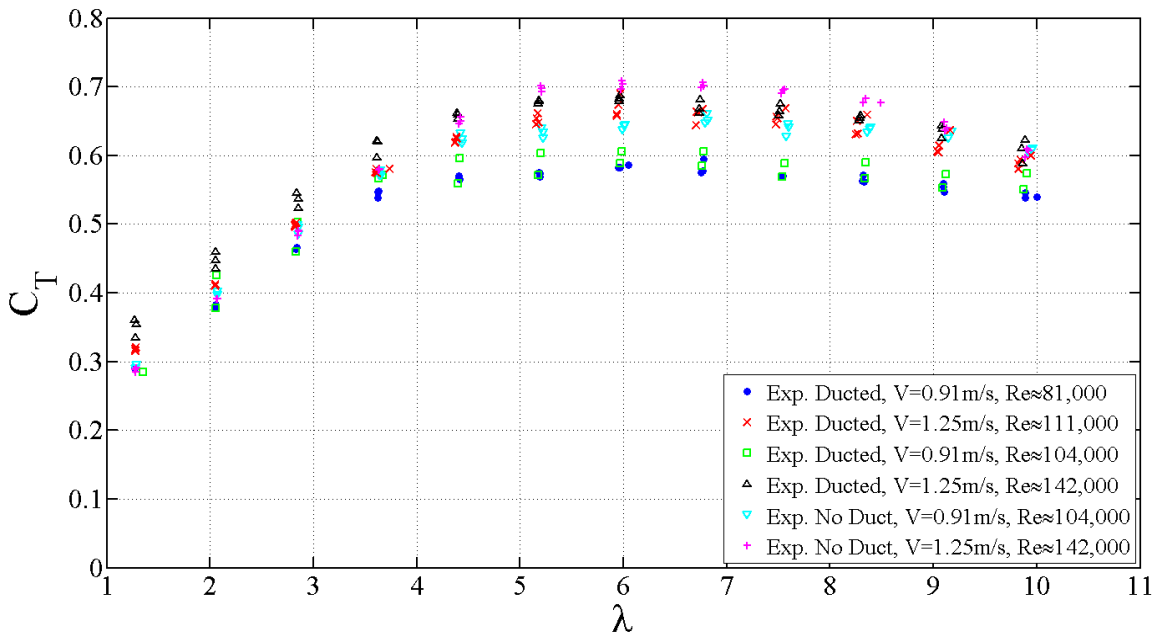

Figure 5.7 C_T vs. tip speed ratio for the ducted turbine without the duct is shown with results of the same rotor without the duct.

CHAPTER 6. DISCUSION AND CONCLUSIONS

This section discusses the results and compares the experimental data to predictions from the OpenProp program for both the free tip and ducted turbines. Several factors were found to play important roles in this testing. They include temperature related Reynolds number effects, blade roughness, uncertainty and repeatability of the instrumentation and duct optimization.

6.1 DISCUSSION

The free tip turbine performed close to predictions but the ducted turbine did not perform as was expected. The underperformance of the ducted turbine may have been a result of inadequate duct lift force. The lack of lift force requires further study but some hints to its possible causes are in the data and will be discussed in the coming sections. Results of C_P for the two turbines are shown in Figure 6.1 and Figure 6.2.

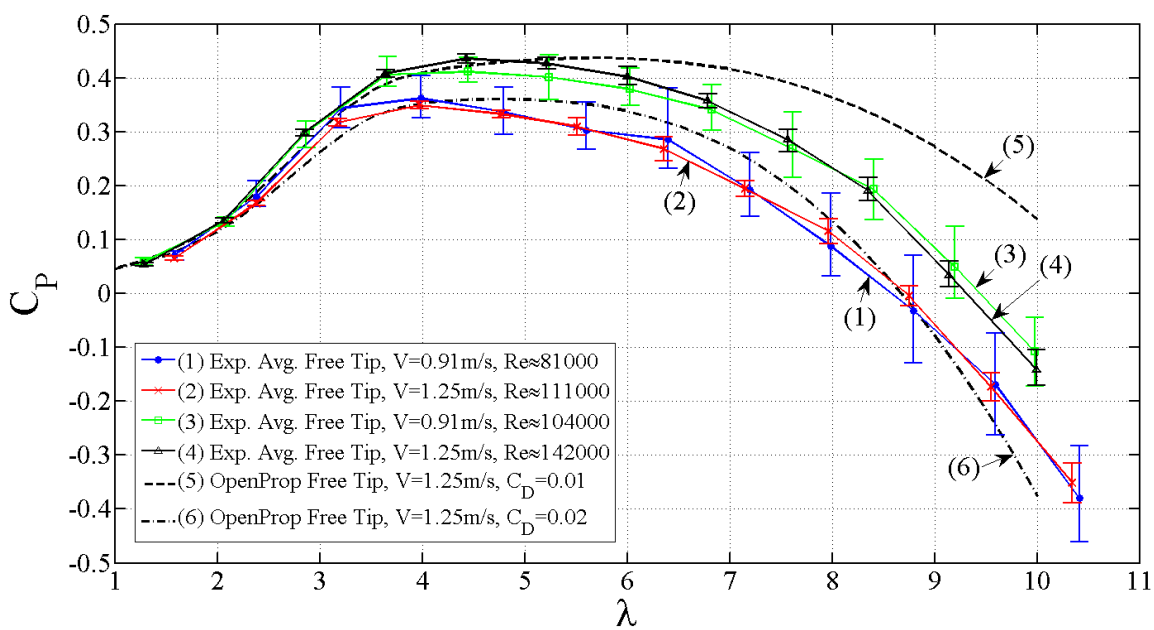

Figure 6.1 Free tip average C_P vs. tip speed ratio is shown for the two carriage speeds. The Reynolds numbers represent the change in both the velocity seen at the blade and water temperature.

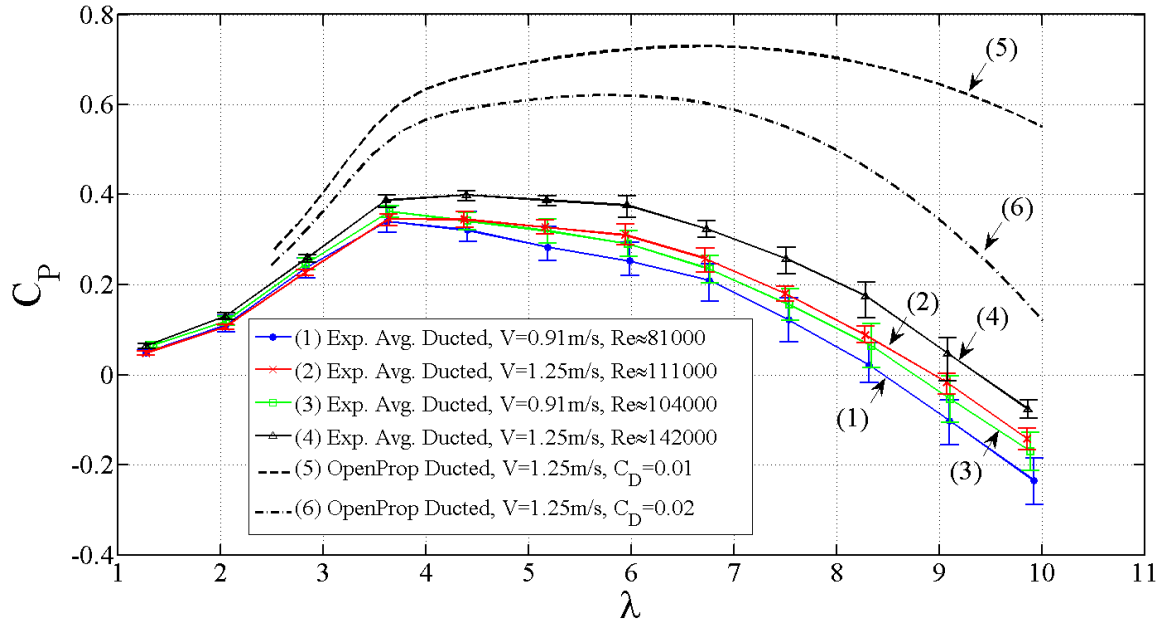

Figure 6.2 Ducted average C_p vs. tip speed ratio is shown for the two carriage speeds. The Reynolds numbers represent the changes in the velocity seen at the blade and in the water temperature.

To more easily see the trends, results in this chapter are displayed as averages with error bars are added to show the quality of the data. Error bars (E) include instrumentation uncertainty (w) and experimental repeatability (Δ). The method used to calculate w and Δ can be found in Appendix E. The error bars were found by combining w and Δ, $E = \sqrt{w^2 + \Delta^2}$.

As discussed in Chapter 5 the acquired data has shown that the Reynolds number has an influence on blade forces [21] [22] which in turn effects C_p and C_T. This explains the variations between OpenProp predictions and experimental data as shown for the free tip case in figure Figure 6.1. This also holds true for the data from the ducted case (Figure 6.2) but with added complication of the duct fluid dynamics.

6.1.1 Reynolds Number and Water Temperature Effects

Reynolds number (Re) effect is an important factor to consider for this scale of testing. It has a major effect on the lift and drag (blade forces) of the turbine. The lift and drag in turn affects the torque and thrust created by the turbine, which are needed to calculate C_p and C_T. For the range of Reynolds numbers shown for this testing ($81000 \lesssim Re \lesssim 142000$) the blades are operating in the transitional range and could be at least partially stalling up to $Re \approx 140000$ thereby reducing performance [21] [22].

The Reynolds numbers displayed for this study are approximations based on common practice and the best information available. The Reynolds numbers were found using $Re = \frac{\rho V^* C}{\mu}$ where $\rho =$ density, V^*= local velocity, C = blade chord length and $\mu =$ viscosity. By convention the chord length and local velocity is taken at r/R = .7 [21][22]. The blade chord length was found from the OpenProp geometry file. V^* for both the free tip and ducted turbine were found using free tip OpenProp code and includes radial, axial and induced velocity components [6].

V^* from the free tip code was used for the ducted turbine since OpenProp over predicts the performance for ducted turbine by more than 50% (Figure 6.2) but comes closer to the experimental performance with the free tip turbine code (Figure 6.1). The velocity for the ducted turbine should therefore be a closer approximation using the free tip code.

The Reynolds number, Re, is highly dependent on the water temperature in the tow tank because of the effect on viscosity, μ, and to a lesser degree on the density, ρ. Water temperature records for the tow tank began in March and do not exist for all of the first set data shown at $Re \approx 81000$ and $Re \approx 111000$. Some of the data for those

Reynolds numbers was taken when the water was colder during the month of January while the rest was taken in March and April when water temperatures were recorded at about 10^0C. The temperature of the water for testing done in January was conservatively estimated to be 10^0C and could have been colder since the ambient temperature was colder in January. Temperature records for the tow tank for later testing at $Re \approx 104000$ and $Re \approx 142000$ show the water at 19.5^0C. The 9.5^0C temperature change accounts for the change in Re at the same inflow velocity (V).

6.1.1.1 Free tip turbine

C_p for the free tip turbine (Figure 6.1) shows reasonably good agreement with OpenProp . The maximum experimental $C_p = .44$ which occurred at the design velocity of $V = 1.25\ m/s$. This compares to the maximum $C_p = .44$ from OpenProp. Results from the lower Reynolds numbers ($Re \approx 81000$ and $Re \approx 11000$) show reasonable correlation with OpenProp predictions and with previous experimental data at $C_D = .02$ [6].

Testing at higher Reynolds number ($Re \approx 104000$ and $Re \approx 142000$) shows an increase in efficiency over the lower Reynolds numbers that could indicate at least part of the turbine is operating in the transition range. The peak experimental data of $C_p = .44$ matches the peak prediction of C_p from OpenProp at $C_D = .01$. The lower drag coefficient is consistent with drag coefficients typically used for marine propeller testing [6]. It is also consistent with published data for marine propellers showing that at least some testing was performed in the transition range [21] [22].

As discussed in Chapter 5 the data in Figure 6.1 for Re ≈ 10400 appears to be higher than expected when compared to $Re \approx 111000$. Increased blade roughness explains this

difference by causing the flow to be moved out of the transitional region thus having the same effect as increasing Reynolds number. This is consistent with published data on wind turbines showing the effects of blade roughness on C_p [23]. A picture of the damaged blade can be seen in Appendix G.

6.1.1.2 Ducted Turbine

Results from the ducted turbine while informative are not as expected. The ducted turbine is affected by the Reynolds number in the same way as the free tip turbine. Curves (1-4) in Figure 6.2 show a trend of increased C_p along with increased Reynolds number. Curve (4) shows the best performance of $C_p = .40$ for the ducted turbine, it also represents the data for the highest Reynolds number. This is well below the predictions of OpenProp. Reynolds number effects and blade roughness do not explain the low performance for the ducted turbine, however some other data collected from this research helps.

6.1.2 Duct Thrust

Some insight to performance of the ducted turbine can be gained from looking at the duct thrust coefficient. As stated in section 2.2, OpenProp does not optimize the duct but provides a duct lift coefficient and inflow angle to aid in duct design. These values are based in part, on the duct thrust coefficient that is entered in OpenProp ($C_{TD} = .2$ as designed). The duct thrust coefficient (Figure 6.3) plays an important role in understanding why ducted C_p falls short of predictions. The duct thrust coefficient (Figure 6.3) shows very little change in experimental C_{TD}, while OpenProp predicts that C_{TD} should rise.

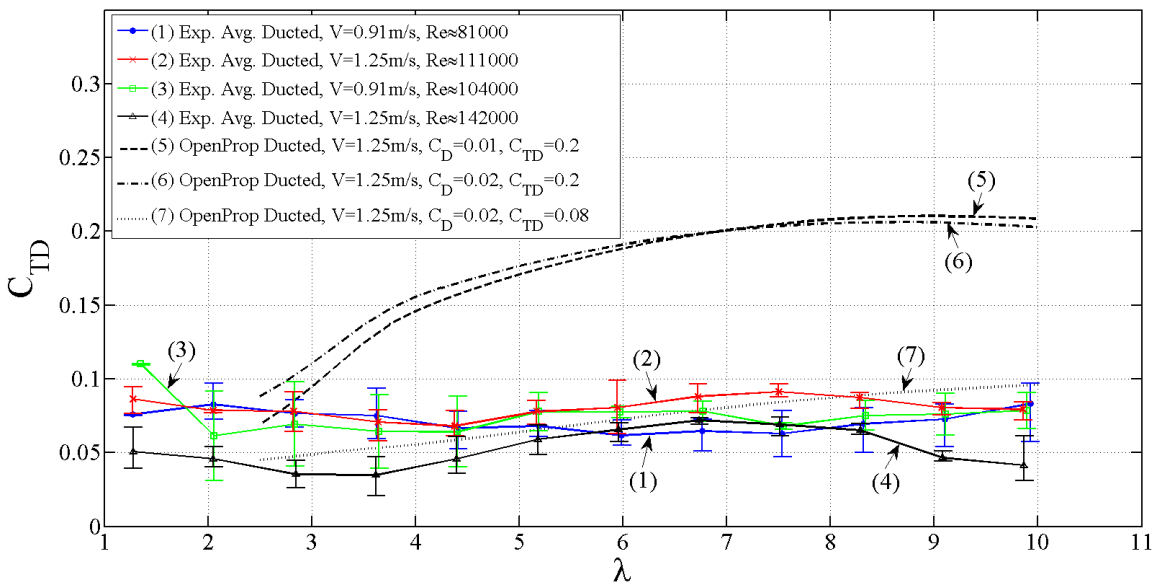

Figure 6.3 Duct thrust coefficient vs. tip speed ratio is shown for the two carriage speeds. The Reynolds numbers represent the changes in the velocity seen at the blade and in the water temperature. OpenProp predictions at $C_D = .01$ and $C_D = .02$ are also shown.

This relatively flat value of $C_{TD} \approx .08$ throughout the range of λ is indicative that the duct is not providing a contributing lift force and that C_{TD} is due only to drag. λ is varied by changing the frequency of the turbine at a given carriage speed (V) which would lead to a constant duct thrust coefficient if the duct produced no lift and C_{TD} was only due to drag. There are several possible causes for the duct to underperform. They include:

- Separation of the boundary layer on the duct caused by an adverse pressure gradient created by the rotor inside the duct [24][18].
- Lower than expected inflow velocity (V^*) to the duct as found by OpenProp.
- Incorrect inflow angle (β_{iD}) to the duct as found by OpenProp.
- Incorrect assumption made about the duct drag coefficient that was entered into OpenProp.

To examine what qualitative affect an incorrect duct drag coefficient would have on duct performance XFoil [15] was used to find the drag coefficient of the duct (C_D). Figure 6.4 shows the range of lift and drag coefficients for the range of Reynolds numbers that the duct might see. At the designed inflow velocity of $= 1.25\ m/s$ $C_D \approx .012$.

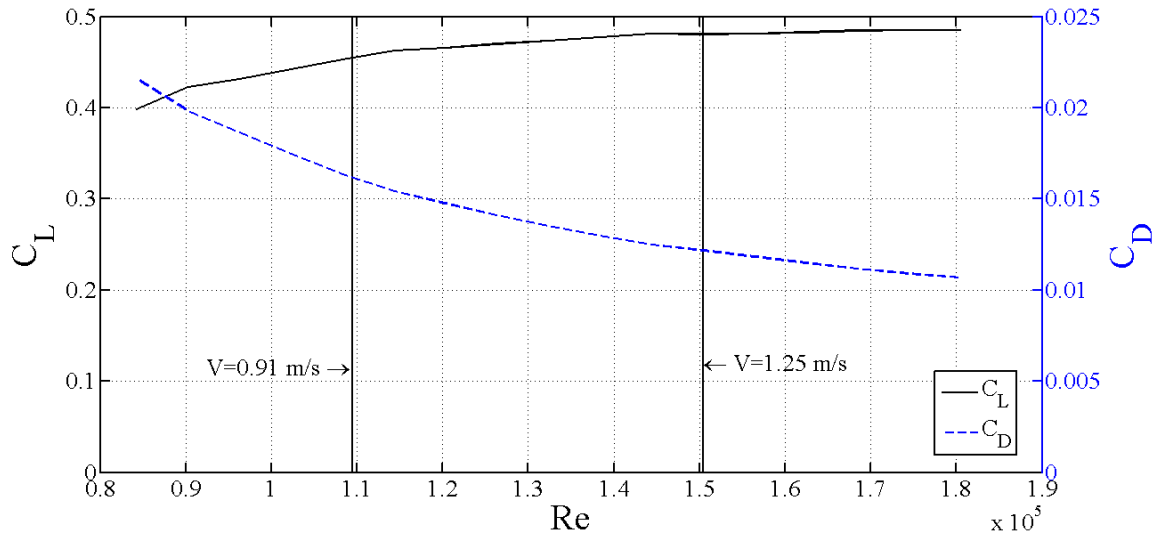

Figure 6.4 C_L & C_D for the duct as a function of Re.

The duct drag coefficient is entered into OpenProp by the user. The design for the duct was done with $C_D = .02$ (see Appendix C). If the value of $C_D = .012$ from XFoil [15] is used as the input to OpenProp it changes the output parameters used in the duct design, as explained in Chapter 2, substantially. The duct lift coefficient changes from $C_{LD} = .5$ to $C_{LD} = .2$ and the duct inflow angle changes from $\beta_{iD} = -1°$ to $\beta_{iD} = 0°$. These parameters substantially change the design of the duct. For instance the importance of β_{iD} can be by examining Figure 6.5 .

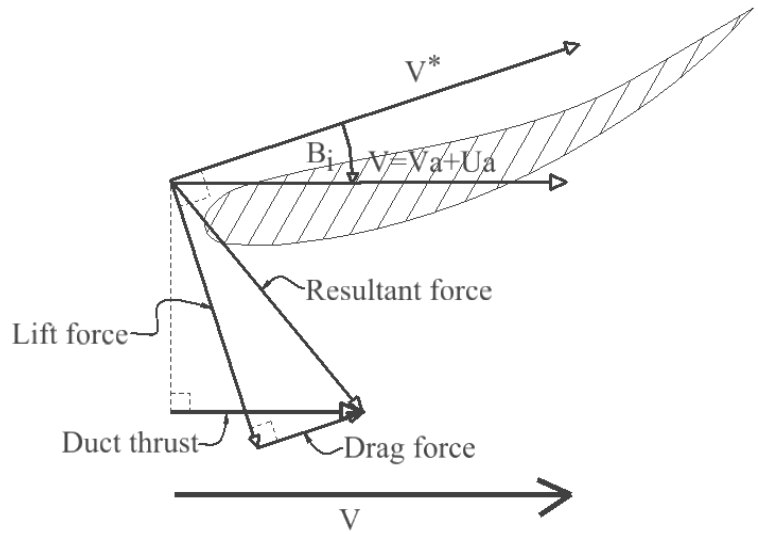

Figure 6.5 This figure shows the upper half of a duct with the relevant force vectors drawn in. It is representative only and is not to scale.

Figure 6.5 shows that the duct lift force acts perpendicular to V^* [25]. If $\beta_{iD} = 0°$ then the lift force would act perpendicular to V and not contribute to the duct thrust as shown in Figure 6.5. This means that the duct thrust coefficient (C_{TD}) would be a function of only drag force and not of lift force leading to a constant C_{TD} as exhibited in Figure 6.3.

6.1.3 OpenProp Validation

Even though the ducted turbine did not perform as expected, it does not necessarily follow that the data is not useful for validation of the ducted turbine in OpenProp. While the design of the duct was not optimal a robust code should work off-design as well as for an optimal design. Given that C_{TD} was provided as an input to OpenProp, an investigation was made to see if OpenProp would predict a more accurate C_p curve if the experimental value of C_{TD} was provided as the input. Figure 6.6 shows OpenProp's prediction of C_p, curve (7), using experimental $C_{TD} = .08$.

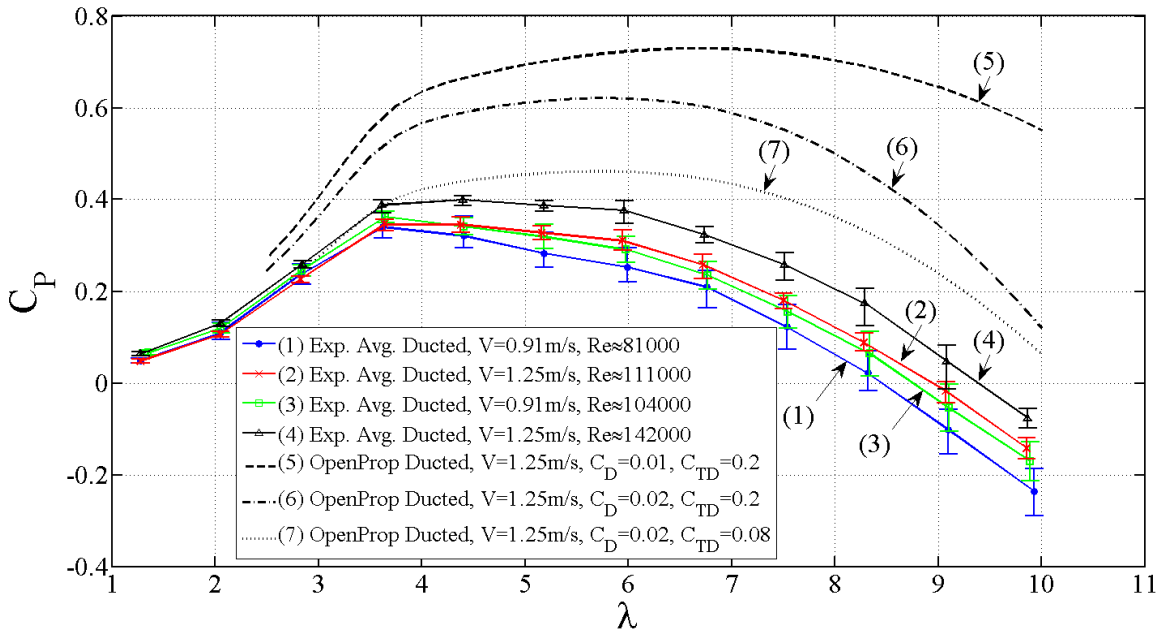

Figure 6.6 Ducted power coefficient vs. tip speed ratio of experimental data and OpenProp predictions. Curve (7) shows C_p from OpenProp adjusted with experimental $C_{TD} = .08$.

Figure 6.6 shows that C_p has a much closer match at low tip speed ratios but is still not a good fit at higher tip speed ratios entering experimental $C_{TD} = .08$ as the input to OpenProp.

It is important to note that currently OpenProp does not provide the ability to analyze existing turbine geometry. For the ducted turbine case the code always optimizes the geometry of the turbine. The difference in the output files for the turbine geometry was examined from $C_{TD} = .2$ to $C_{TD} = .08$ and found to be very small. So, curve (7) is an approximation but is a reasonable one.

6.1.4 Free Tip and Ducted C_T Discussion

The average thrust coefficients with uncertainty bars for the free tip and ducted turbines are shown below in Figure 6.7 and Figure 6.8. These figures do not agree well

with OpenProp for either case but are consistent with the Reynolds number effects discussed in this chapter. Figure 6.8 also includes OpenProp's prediction using the experimental value of $C_{TD} = .08$ as input. No published data for thrust coefficients of marine turbines could be found for comparison purposes.

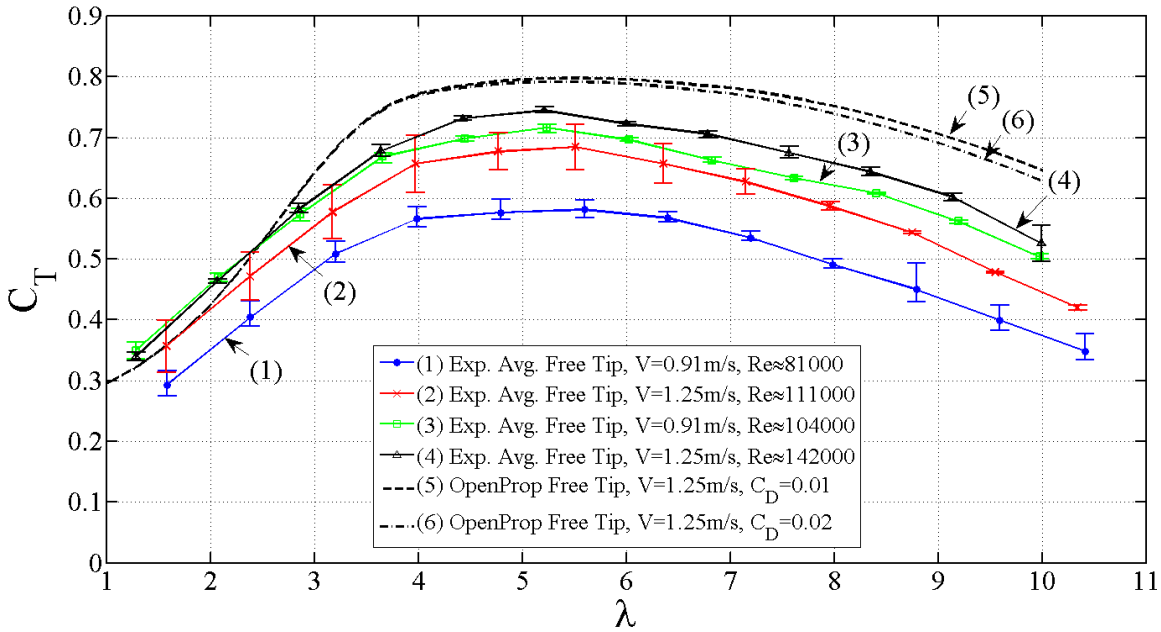

Figure 6.7 Free tip average C_T vs. tip speed ratio is shown for the two carriage speeds. The Reynolds numbers represent the changes in the velocity seen at the blade and in the water temperature.

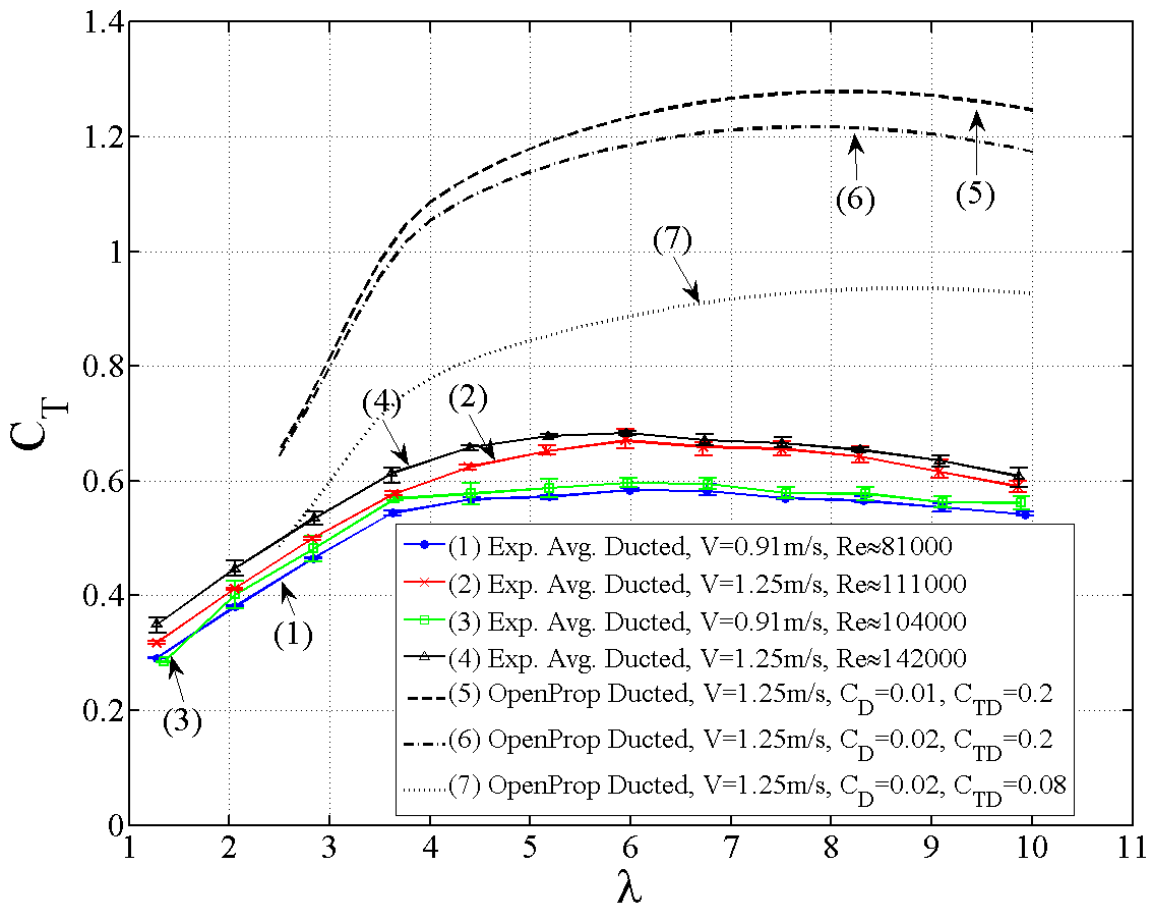

Figure 6.8 Ducted average C_T vs. tip speed ratio is shown for the two carriage speeds. The Reynolds numbers represent the changes in the velocity seen at the blade and in the water temperature. OpenProp prediction with $C_{TD} = .08$ is added for comparison.

6.2 CONCLUSIONS

A free tip and ducted turbine was designed, built and tested at a range of tip speed ratios of $1 \lesssim \lambda \lesssim 10$ for two inflow velocities $V = .91\ m/s$ and $V = 1.25\ m/s$. The free tip turbine performed as expected with a maximum C_p= .44, the same as OpenProp's prediction of maximum C_p= .44. This is consistent with published data on the free tip turbine designed with OpenProp [26] and provides a benchmark against which to check both the design method and testing procedure. The overall power coefficient obtained

from the ducted turbine reached a maximum of C_p= .40. The measured C_p is considerably lower than the C_p= .65 predicted with OpenProp. The ducted turbine was also tested with the duct removed and displayed very little change in C_p when compared to tests performed with the duct in place (Figure 5.6).

The primary goal of this thesis was to provide ducted axial flow tidal turbine data for other researchers to validate numerical design codes against. This goal has been met by providing C_P, C_T and C_{TD} for a range of Reynolds numbers and inflow velocities as shown in Figure 5.3, Figure 5.4 and Figure 5.5 respectively.

Both turbines exhibited performance changes based on Reynolds number by showing higher values of C_P with at higher Reynolds numbers. This is consistent with published data showing that the turbines are operating in the transitional region at this scale of testing and Reynolds number effects as well as blade roughness play an important role in performance [27] [28] . Water temperature played a significant role in performance because Reynolds numbers is a function of temperature.

The duct did not perform as expected and had very little impact on turbine performance. Examination of the duct thrust coefficient provides some insight into why the duct did not perform as expected by displaying a nearly constant value of $C_{TD} \approx .08$ throughout the range of tip speed ratios. The nearly constant value of the duct thrust indicates that the duct is not providing the lift component that contributes to the duct thrust. In the absence of a lift component the duct does not increase the C_P. No specific cause for the lack of lift was determined but several possibilities explanations are presented in Chapter 6.

The fact that the data for the free tip model matches OpenProp reasonably well suggests that the approach to taking the data is a reasonable way to validate the code. OpenProp should prove to be a useful design tool for free tip turbines. Data for the ducted turbine demonstrates the challenges associated with designing a ducted turbine. Continuing development of OpenProp is needed in order for the code to be useful for ducted turbine designs. Further validation with optimized ducts will also be needed prior to making extensive use of the design code.

6.3 FUTURE WORK

There are several areas that could be improved in modeling and testing. The ones this author suggests beginning with are stated below, in no particular order of importance.

6.3.1 Experimental

The turbine test platform requires carefully calibration for frictional losses. Some of the measured values for this testing are very small, in some cases much smaller than the frictional loss, i.e., the measured torque is smaller than the tare. This correction is inherently difficult. A new test platform should be developed to minimize friction from the experimental setup. The new platform should be designed to use a dry hub and a six-axis load cell. A control motor in line with the shaft will minimize the number of parts but will introduce additional seal problems. However, assuming that a proper shaft seal can be found this system should produce more repeatable results.

6.3.2 Modeling

The modeling of the ducted turbine in OpenProp has not been previously validated. Some areas that the ducted turbine model could benefit from include:

- Implement tip gap model
- Implement duct optimization routine
- Implement a function for ducted turbines to analyze existing geometry for off-design conditions
- The design tip speed ratio for the testing in this thesis is $\lambda = 7$. For both the free tip and ducted cases the maximum power coefficient occurs between $\lambda = 4$ and $\lambda = 5$; this is also supported by previous work [26]. This critical aspect of the turbine design is also in need of additional work in the model

WORKS CITED

[1] [Online]. Available: http://www.marineturbines.com/. [Accessed 4 June 2012].

[2] A. J. W. B. A.S. Bahaj, "Power and thrust measurements of marine current turbines under various hydrodynamic flow conditions in a cavitatoin tunner and towing tank," *RENEWABLE ENERGY*, 2005.

[3] B. Kirke, "Developments in Ducted Water Current Turbines," www.cyberaid.net, Sustainable Energy Centre, University of South Australia, Mawson Lakes, SA 5095, Austrailia, 2003.

[4] G. S. deBree, "Testing and Modeling of High Solidity Cross-Flow Tidal Turbines," University of Maine, Orono, Maine, 2012.

[5] *Labview, National Instruments,* North Mopac Expressway, Austin, TX 78759.

[6] B. P. Epps, "PhD Thesis, An Impulse Framework for Hydrodynamic Force Analysis:," MIT, Cambride, MA, 2010.

[7] J. W. Ketchum, "Design, Build and Test of an Axial Flow Hydrokenetic Turbine with Fatigue Analysis," MIT, Cambride, MA, 2010.

[8] R. Kimball, ""OpenProp v2.4 Propeller/Turbine Design Code," http://openprop.mit.edu, 2010.," [Online]. Available: http://openprop.mit.edu/~openprop/wiki/index.php?title=Main_Page. [Accessed 11 January 2012].

[9] *Mathworks, Natick MA. USA.*

[10] W. B. Coney, "A Method for the Design of A Class of Optimum Marien Propulsors," MIT, Cabridge, MA, 1989.

[11] J. M. Stubblefield, "Numerically-Based Ducted Propeller Design," MIT, Cabridge, MA, 2008.

[12] *Marine Current Turbines Limited, Stoke Gifford, Bristol, UK.*

[13] *Siemens AG, Munich, Germany.*

[14] V. B. H. Schneekluth, Ship Design for Efficiency and Economy, Oxford, UK: Butterworth-Heinemann, 1998.

[15] M. Drela, "XFOIL," [Online]. Available: http://web.mit.edu/drela/Public/web/xfoil/. [Accessed 8 June 2012].

[16] *Dassault Systèmes SolidWorks Corporation,* 175 Wyman Street, Waltham, MA 02451.

[17] *Parker Hannifin Corporation,* Rohnert Park, CA..

[18] R. Kimball, *Personal Communication,* June 2012.

[19] R. W. Kimball, "Experimental Investigation and Numerical Modelling of a Mixed Flow Marine Waterjet; Ph.D. Thesis," Massachusetts Institute of Technology, Cambridge MA, 2001.

[20] S. L. B. S. V. M. F. M. C. F. Gaggero Stefano, "Comparison of experimental measurements and numerical calculations for a propellor in axial cylinder," in *First International Symposium on Marine Propulsors*, Trodheim, Norway, 2009.

[21] P. L. Troost, "Reynolds Number for Model Propeller Experiments," Netherlands Model Basin, 1948.

[22] M. A.-M. G. H. Sven-Brian Muller, "Scale Effects on Propellers for Large Container Vessels," in *First Internatioal Symposium on Marine Propulsors*, Trondheim, Norway, June 2009.

[23] H. R. Martin, "Development of a Scale Model Wind Turbine for Testing of Offshore Floating Wind Turbine Systems," University Of Maine, Orono, Maine, 2011.

[24] B. Epps, *Personal Communication,* June 2012.

[25] J. E. Kerwin, *13.04 Lecture Notes, Hydrofoils and Propellers,* MIT, 2001.

[26] B. P. Epps, “PhD Thesis, An impulse framework for hydrodynamic force analysis:,” MIT, Cambride, MA, 2010.

[27] P. L. Troost, “Reynolds Number for Model Propeller Experiments,” Netherlands Model Basin, 1948.

[28] M. A.-M. G. H. Sven-Brian Muller, “Scale effects onpropellers for large container vessels,” in *First Internatioal Symposium on Marine Propulsors*, Trondheim, Norway, June 2009.

[29] J. P. Holman, Experimental Methods for Engineers, McGraw-Hill, 2007.

[30] W. B. Coney, "A Method for the Design of A Classs of Optimum Marine Propulsors," MIT, 1989.

[31] M. R. Shives, "Hydrodynamic Modeling, Optimization and Performance Assesment for Ducted and Non-Ducted Tidal Turbines," Carleton University, 2008.

[32] G. P. M. Hugh, "Advances in Ducted Propulsor Analysis using Vortex-Lattice Lifting-Surface Techniques," MIT, 1997.

APPENDIX A: FREE TIP INPUT CODE

```
Using OpenProp V2.4.4
% ------------------------------------------------------------ Example_input.m
% Created: 3/2/2010, Brenden Epps, bepps@mit.edu
%
% This script creates an "input" data structure for use in OpenProp.
%
% To design a propeller using these inputs, run:
%                                    design = EppsOptimizer(input)
%
% ---------------------------------------------------------------------------
clear, %close all, clc

filename   = 'OpenProp Tom unducted Aug_11_2012';   % filename prefix
notes      = 'Ducted propeller from Sutbblefield (2008) M.S. thesis';

% ------------------------------------------------------------ Design parameters
Z        = 3;            % number of blades
% N        = 72*(60/2/pi); % propeller speed [RPM]
N=650;
D        = 0.254;         % (approx 10 in) propeller diameter [m] (Note: 39.37 in/m )

THRUST    = 0;            % (11.240 lb) required thrust [N] (0.2248 lb/N)
% Vs       = .915;%1.25;            % ship velocity [m/s]
Vs       = 1.25;
Dhub      = .04445;       % hub diameter [m] (must be greater than 0.15*D)

Mp        = 20;           % number of vortex panels over the radius
Np        = 20;           % number of points along the chord
ITER      = 75;           % number of iterations in wake alignment
Rhv       = 0.5;          % hub vortex radius / hub radius
HUF       = 0;            % Hub Unloading Factor (0 == no unloading, 1 == reduced loading)
TUF       = 0;            % Tip Unloading Factor (0 == no unloading, 1 == reduced loading)
SCF       = 1;            % Swirl Cancellation Factor (1 == no cancellation)
rho       = 1000;         % water density [kg/m^3]

H        = 1;             % Shaft centerline depth [m]
dV        = 0.2;          % Inflow variation [m/s]
Np        = 20;           % Number of points over the chord for geometry plots [ ]



% ------------------------------------------------------------ Duct parameters
% Inputs for no duct: Duct_flag = 0; TAU = 1; Rduct_oR = 1; CDd = 0;
TAU        =.9;          % thrust ratio
Rduct      = D/2;          % duct radius [m]
Cduct      = D/3;          % duct chord length [m]
CDd        = 0.008;        % duct viscous drag coefficient


% ---------------------------------------------- Blade 2D section properties
Meanline   = 'NACA a=0.8';          % Meanline type  (1 == NACA a=0.8, 2 == parabolic)
Thickness  = 'NACA 65A010';          % Thickness form (1 == NACA 65A010, 2 == elliptical, 3 ==
parabolic)
```

```
alphaI     = 1.54;        % [deg] ideal angle of attack  (should match with Meanline type)
CLI        = 1.0;        % [ ],  ideal lift coefficient (should match with Meanline type)


XR         = [0.2    0.3    0.4    0.5    0.6    0.7    0.8    0.9    0.95   1.0];    % radius / propeller radius
XCoD       = [0.1600 0.1818 0.2024 0.2196 0.2305 0.2311 0.2173 0.1806...
              0.1387 0.000001]; % chord / diameter unducted

% XCoD       = [0.2600 0.2321 0.2109 0.1957 0.1900 0.1845 0.1800 0.1800 0.1800 0.1800]; %(old) chord /
diameter ducted
XCD        = .02;%[0.0080 0.0080 0.0080 0.0080 0.0080 0.0080 0.0080 0.0080 0.0080 0.0080]; % section
drag coefficient
% XCD        = [0.18 0.018 0.018 0.018 0.0180 0.01800 0.0180 0.01800 0.01800 0.01800];
XVA        = [1      1      1      1      1      1      1      1      1      1      ]; % axial      inflow velocity / ship velocity
XVT        = [0      0      0      0      0      0      0      0      0      0      ]; % tangential inflow velocity / ship velocity
t0oc0      = [0.2056 0.1551 0.1181 0.0902 0.0694 0.0541 0.0419 0.0332 0.0324 0.0000]; % max section
thickness / chord
skew0      = [0      0      0      0      0      0      0      0      0      0      ]; % skew [deg]
rake0      = [0      0      0      0      0      0      0      0      0      0      ]; % rake / diameter


% ------------------------------------------------------------------ Flags
Propeller_flag  = 0;      % 0 == turbine, 1 == propeller
  Viscous_flag  = 1;      % 0 == viscous forces off (CD = 0), 1 == viscous forces on
      Hub_flag  = 1;      % 0 == no hub, 1 == hub
     Duct_flag  = 0;      % 0 == no duct, 1 == duct
     Wake_flag  = 0;      % 0 == Horseshoe(...,Wrench(...)), 1 == Wake_Horseshoe(...)
     Plot_flag  = 1;      % 0 == do not display plots, 1 == display plots
    Chord_flag  = 1;      % 0 == do not optimize chord lengths, 1 == optimize chord lengths
Optimizer_flag  = 2;      % 1 == Lerbs optimizer, 2 == Epps optimizer
 Lagrange_flag  = 0;      % 0 == do not fix Lagrange multiplier, 1 == fix Lagrange multiplier

LM0     = -1;     % [1 x 1] fixed value of Lagrange multiplier

Make2Dplot_flag = 1; % 0 == do not make a 2D plot of the results, 1 == make plot
Make3Dplot_flag = 1; % 0 == do not make a 3D plot of the results, 1 == make plot
Make_Rhino_flag = 0; % 0 == do not make Rhino files, 1 == make Rhino files
% ---------------------------------------------- Compute derived quantities
n       = N/60;                    % revolutions per second [rps]
R       = D/2;                     % propeller radius [m]
Rhub    = Dhub/2;                  % hub radius [m]
Rhub_oR = Rhub/R;
Js      = Vs/(n*D);                % advance coefficient
L       = pi/Js;                   % tip-speed ratio
CTDES   = THRUST/(0.5*rho*Vs^2*pi*R^2); % CT thrust coefficient required

dVs     = dV/Vs;                   % axial inflow variation / Vs
CDoCL   = mean(XCD)/CLI;


ALPHAstall = 8*pi/180;  % [rad], stall angle of attack - ideal angle of attack
dCLdALPHA  = 2*pi;      % d(CL)/d(alpha)

% ========================================================================
% ================================================= Pack up input variables
input.filename   = filename;    % filename prefix for output files
```

```
input.date       = date;        % today's date

input.part1      = '------ Performance inputs ------';
input.Z          = Z;           % [1 x 1], [ ] number of blades
input.N          = N;           % propeller speed [RPM]
input.D          = D;           % propeller diameter [m]
input.Vs         = Vs;          % [1 x 1], [m/s] ship speed
input.Js         = Js;          % [1 x 1], [ ] advance coefficient, Js = Vs/nD = pi/L
input.L          = L            % [1 x 1], [ ] tip speed ratio, L = omega*R/V
input.THRUST     = THRUST;      % required thrust [N]
input.CTDES      = CTDES;       % [1 x 1], [ ] desired thrust coefficient

input.part2      = '------ Geometry inputs ------';
input.Mp         = Mp;          % [1 x 1], [ ] number of blade sections
input.Np         = Np;          % [1 x 1], [ ] number of points along the chord
input.R          = R;           % [1 x 1], [m] propeller radius
input.Rhub       = Rhub;        % [1 x 1], [m] hub radius
input.XR         = XR;          % [length(XR) x 1], [ ] input radius/propeller radius
input.XVA        = XVA;         % [length(XR) x 1], [ ] input axial inflow velocity  at XR
input.XVT        = XVT;         % [length(XR) x 1], [ ] input swirl inflow velocity  at XR
input.XCD        = XCD;         % [length(XR) x 1], [ ] input drag coefficient       at XR
input.XCoD       = XCoD;        % [length(XR) x 1], [ ] input chord / diameter       at XR
input.t0oc0      = t0oc0;       % [length(XR) x 1], [ ] input thickness / chord      at XR
input.skew0      = skew0;       % [length(XR) x 1], [ ] input skew  [deg]      at XR
input.rake0      = rake0;       % [length(XR) x 1], [ ] input rake X/D       at XR
input.Meanline   = Meanline;    % 2D section meanline  flag
input.Thickness  = Thickness;   % 2D section thickness flag
input.ALPHAstall = ALPHAstall;  % [rad], stall angle of attack - ideal angle of attack
input.alphaI     = alphaI;      % [1 x 1], [deg] input ideal angle of attack  at XR
input.dCLdALPHA  = dCLdALPHA;   % d(CL)/d(alpha)
input.CLI        = CLI;         % [1 x 1], [ ] input ideal lift coefficient at XR
input.CDoCL      = CDoCL;       % [1 x 1], [ ] blade section drag coefficient / lift coefficient

input.part3      = '------ Computational inputs ------';
input.ITER           = ITER;          % [ ] number of iterations
input.Propeller_flag  = Propeller_flag; % 0 == turbine, 1 == propeller
input.Viscous_flag    = Viscous_flag;   % 0 == viscous forces off (CD = 0), 1 == viscous forces on
input.Hub_flag        = Hub_flag;       % 0 == no hub, 1 == hub
input.Duct_flag       = Duct_flag;      % 0 == no duct, 1 == duct
input.Plot_flag       = Plot_flag;      % 0 == do not display plots, 1 == display plots
input.Chord_flag      = Chord_flag;     % 0 == do not optimize chord lengths, 1 == optimize chord lengths
input.Wake_flag       = Wake_flag;      % 0 == Horseshoe(...,Wrench(...)), 1 == Wake_Horseshoe(...)
input.Optimizer_flag  = Optimizer_flag; % 1 == Lerbs optimizer, 2 == Epps optimizer
input.Lagrange_flag   = Lagrange_flag;  % 0 == do not fix Lagrange multiplier, 1 == fix Lagrange
multiplier
input.Make2Dplot_flag = Make2Dplot_flag;
input.Make3Dplot_flag = Make3Dplot_flag;
input.Make_Rhino_flag = Make_Rhino_flag;
input.LM0        = LM0;         % [1 x 1] fixed value of Lagrange multiplier
input.HUF        = HUF;         % [1 x 1], [ ] Hub Unloading Factor (0 == no unloading, 1 == reduced
loading)
input.TUF        = TUF;         % [1 x 1], [ ] Tip Unloading Factor (0 == no unloading, 1 == reduced loading)
input.SCF        = SCF;         % [1 x 1], [ ] Swirl Cancellation Factor (1 == no cancellation)
input.Rhv        = Rhv;         % [1 x 1], [ ] hub vortex radius / hub radius

input.part4      = '------ Cavitation inputs ------';
```

```
input.rho       = rho;        % [1 x 1], [kg/m^3] fluid density
input.dVs       = dVs;        % [1 x 1], [ ] ship speed variation / ship speed
input.H         = H;          % [1 x 1]

input.part5     = '------ Duct inputs ------';
input.TAU       = TAU;        % [1 x 1], [ ] propeller thrust / total thrust
input.Rduct     = Rduct;      % [1 x 1], [m] duct radius
input.Cduct     = Cduct;      % [1 x 1], [m] duct chord length
input.CDd       = CDd;        % [1 x 1], [ ] duct drag coefficient


% ---------------------------- Pack up propeller/turbine data structure, pt
pt.name     = filename; % (string) propeller/turbine name
pt.date     = date;     % (string) date created
pt.notes    = notes;    % (string or cell matrix)   notes
pt.input    = input;    % (struct) input parameters
pt.design   = [];       % (struct) design conditions
pt.geometry = [];       % (struct) design geometry
pt.states   = [];       % (struct) off-design state analysis

% ------------------------------------------------------------ Save input data
save OPinput pt input

clear, clc,
pause(0.01),
pause(0.01),

load OPinput,

pause(0.01),
pause(0.01),

input
```

APPENDIX B: FREE TIP BLADE GEOMETRY FILE

OpenProp Tom unducted Aug_11_2012_Geometry.txt

Propeller Geometry Table

Date and time: 11-Jun-2012

Propeller Diameter = 0.2540 m
Number of Blades = 3
Propeller Speed = 650 RPM
Propeller Hub Diameter = 0.0445 m
Meanline Type: NACA a=0.8
Thickness Type: NACA 65A010

r/R	P/D	Skew	Xs/D	c/D	f0/c	t0/c
0.1954	0.2716	0.0000	0.0000	0.1597	-0.0350	0.2193
0.2361	0.2861	0.0000	0.0000	0.1370	-0.0333	0.2317
0.2769	0.2894	0.0000	0.0000	0.1209	-0.0317	0.2372
0.3176	0.2902	0.0000	0.0000	0.1093	-0.0300	0.2363
0.3583	0.2902	0.0000	0.0000	0.1008	-0.0284	0.2297
0.3991	0.2901	0.0000	0.0000	0.0946	-0.0268	0.2179
0.4398	0.2900	0.0000	0.0000	0.0901	-0.0253	0.2026
0.4806	0.2902	0.0000	0.0000	0.0869	-0.0238	0.1851
0.5213	0.2905	0.0000	0.0000	0.0847	-0.0224	0.1668
0.5620	0.2910	0.0000	0.0000	0.0832	-0.0211	0.1483
0.6028	0.2915	0.0000	0.0000	0.0821	-0.0199	0.1299
0.6435	0.2921	0.0000	0.0000	0.0810	-0.0187	0.1131
0.6843	0.2926	0.0000	0.0000	0.0794	-0.0177	0.0991
0.7250	0.2930	0.0000	0.0000	0.0767	-0.0167	0.0878
0.7657	0.2934	0.0000	0.0000	0.0724	-0.0159	0.0797
0.8065	0.2937	0.0000	0.0000	0.0659	-0.0152	0.0763
0.8472	0.2939	0.0000	0.0000	0.0568	-0.0146	0.0707
0.8880	0.2940	0.0000	0.0000	0.0477	-0.0142	0.0535
0.9287	0.2941	0.0000	0.0000	0.0406	-0.0138	0.0296
0.9694	0.2942	0.0000	0.0000	0.0364	-0.0136	0.0085

r/R [ ], radial position of control points / propeller radius.
P/D [ ], section pitch / diameter.
c/D [ ], section chord-length / diameter.
fo/C [ ], section camber / section chord-length.
to/C [ ], section thickness / section chord-length.

APPENDIX C: DUCTED INPUT CODE

```
Using OpenProp V3.2.0
% ---------------------------------------------------------------------
% Ducted turbine design example:
% ---------------------------------------------------------------------

% ---------------------------------------------------------------------
clear, close all, clc,

filename   = 'turbine';   % filename prefix
notes      = 'Tom Lokocz ducted turbine';

% ---------------------------------------------------------------------
i.part1      = '------ Performance inputs ------';

i.Z        = 3;          % number of blades
i.N        = 650;          % propeller speed [RPM]
i.Vs       = 1.25;            % free-stream speed [m/s]

i.D        = 0.254;         % rotor diameter [m] (Note: 39.37 in/m )
i.Dhub     = .04445;       % hub diameter [m] (must be greater than 0.15*D)

i.L        = pi*(i.N/60)*i.D/i.Vs;                    % tip-speed ratio

% ---------------------------------------------------------------------
input.part2      = '------ Geometry inputs ------';
i.Mp       = 20;           % number of vortex panels over the radius

i.XR       = [0.2    0.3    0.4    0.5    0.6    0.7    0.8    0.9    0.95   1.0];    % radius / propeller radius

% XCoD      = [0.1600 0.1818 0.2024 0.2196 0.2305 0.2311 0.2173 0.1806 0.1387 0.000001]; % chord /
diameter unducted
i.XCoD      = [0.1600 0.1818 0.2024 0.2196 0.2305 0.2311 0.2173 0.19 0.17 0.15]; %(use this one) chord /
diameter ducted
% XCoD      = [0.2600 0.2321 0.2109 0.1957 0.1900 0.1845 0.1800 0.1800 0.1800 0.1800]; %(old) chord /
diameter ducted

i.XCD       = .02;%[0.0080 0.0080 0.0080 0.0080 0.0080 0.0080 0.0080 0.0080 0.0080 0.0080]; % section
drag coefficient
i.XVA       = [1     1     1     1     1     1     1     1     1     1     ]; % axial     inflow velocity / ship velocity
i.XVT       = [0     0     0     0     0     0     0     0     0     0     ]; % tangential inflow velocity / ship
velocity
i.t0oc0     = [0.2056 0.1551 0.1181 0.0902 0.0694 0.0541 0.0419 0.0332 0.0324 0.0000]; % max section
thickness / chord
i.skew0     = [0     0     0     0     0     0     0     0     0     0     ]; % skew [deg]
i.rake0     = [0     0     0     0     0     0     0     0     0     0     ]; % rake / diameter

i.Meanline   = 'NACA a=0.8';          % Meanline type  (1 == NACA a=0.8, 2 == parabolic)
i.Thickness  = 'NACA 65A010';          % Thickness form (1 == NACA 65A010, 2 == elliptical, 3 ==
parabolic)

i.ALPHAstall = 8*pi/180;  % [rad], stall angle of attack - ideal angle of attack
i.dCLdALPHA  = 2*pi;      % d(CL)/d(alpha)
```

```
i.XCLmax = .5;

% ---------------------------------------------------------------------------
i.part3      = '------ Computational inputs ------';

i.Propeller_flag  = 0;      % 0 == turbine, 1 == propeller
  i.Viscous_flag  = 1;      % 0 == viscous forces off (CD = 0), 1 == viscous forces on
      i.Hub_flag  = 1;      % 0 == no hub, 1 == hub
     i.Duct_flag  = 1;      % 0 == no duct, 1 == duct
     i.Plot_flag  = 1;      % 0 == do not display plots, 1 == display plots
    i.Chord_flag  = 1;      % 0 == do not optimize chord lengths, 1 == optimize chord lengths

i.ITER      = 50;           % number of iterations in wake alignment



% ---------------------------------------------------------------------------
i.part4      = '------ Duct inputs ------';
i.Rduct      = i.D/2;%+.00159;          % duct radius [m]
i.Cduct      = i.D/2;          % duct chord length [m]
i.Xduct      = i.Cduct*.25;              % duct axial displacement downstream [m]
i.CDd        = .02;%0.008;        % duct viscous drag coefficient
i.CTD        = -0.2;          % duct thrust coefficient



% ---------------------------------------------------------------------------
i.part5      = '------ Cavitation inputs ------';
i.rho        = 1000;          % water density [kg/m^3]
i.H          = 1;             % Shaft centerline depth [m]
i.dV         = 0.2;           % Inflow variation [m/s]


% ===========================================================================
% ---------------------------- Pack up propeller/turbine data structure, pt
pt.name     = filename; % (string) propeller/turbine name
pt.date     = date;     % (string) date created
pt.notes    = notes;    % (string or cell matrix)   notes
pt.i        = i;        % (struct) input parameters
pt.d        = [];       % (struct) design conditions
pt.g        = [];       % (struct) design geometry
pt.s        = [];       % (struct) off-design state analysis

% ------------------------------------------------------------ Save input data
save OPinput pt

clear, clc,
pause(0.01),
pause(0.01),

load OPinput pt

pause(0.01),
pause(0.01),

pt.i
```

APPENDIX D: DUCTED BLADE GEOMETRY FILE

Date and time: 15-Apr-2012

Propeller Diameter = 0.2540 m
Number of Blades = 3
Propeller Speed = 650 RPM
Propeller Hub Diameter = 0.0445 m
Meanline Type: NACA a=0.8
Thickness Type: NACA 65A010

r/R	P/D	Skew	Xs/D	c/D	f0/c	t0/c
0.1750	0.2859	0.0000	0.0000	0.1855	-0.0340	0.1840
0.2397	0.3054	0.0000	0.0000	0.1509	-0.0340	0.2053
0.3041	0.3126	0.0000	0.0000	0.1282	-0.0340	0.2186
0.3676	0.3165	0.0000	0.0000	0.1112	-0.0340	0.2271
0.4299	0.3190	0.0000	0.0000	0.0982	-0.0340	0.2307
0.4907	0.3207	0.0000	0.0000	0.0880	-0.0340	0.2293
0.5495	0.3220	0.0000	0.0000	0.0799	-0.0340	0.2239
0.6061	0.3233	0.0000	0.0000	0.0734	-0.0340	0.2149
0.6599	0.3245	0.0000	0.0000	0.0682	-0.0340	0.2035
0.7108	0.3257	0.0000	0.0000	0.0640	-0.0340	0.1895
0.7584	0.3270	0.0000	0.0000	0.0605	-0.0340	0.1730
0.8023	0.3285	0.0000	0.0000	0.0577	-0.0340	0.1567
0.8424	0.3300	0.0000	0.0000	0.0553	-0.0340	0.1408
0.8784	0.3316	0.0000	0.0000	0.0533	-0.0340	0.1272
0.9101	0.3328	0.0000	0.0000	0.0517	-0.0340	0.1196
0.9372	0.3339	0.0000	0.0000	0.0503	-0.0340	0.1152
0.9596	0.3355	0.0000	0.0000	0.0492	-0.0340	0.0954
0.9772	0.3372	0.0000	0.0000	0.0483	-0.0340	0.0667
0.9898	0.3386	0.0000	0.0000	0.0476	-0.0340	0.0427
0.9975	0.3397	0.0000	0.0000	0.0472	-0.0340	0.0280
1.0000	0.3400	0.0000	0.0000	0.0471	-0.0340	0.0232

r/R [ ], radial position of control points / propeller radius.
P/D [ ], section pitch / diameter.
c/D [ ], section chord-length / diameter.
fo/C [ ], section camber / section chord-length.
to/C [ ], section thickness / section chord-length.

APPENDIX E: UNCERTAINTY AND REPEATABILITY

Uncertainty and repeatability in instrumentation were calculated as follows. The uncertainty in C_p, C_t and λ were calculated using a MATLAB [9] function written by deBree [4], $w_R = \sqrt{\left(\frac{\partial R}{\partial x_1}\right)^2 w_{x_1}{}^2 + \left(\frac{\partial R}{\partial x_2}\right)^2 w_{x_2}{}^2 + \left(\frac{\partial R}{\partial x_3}\right)^2 w_{x_3}{}^2 + \ldots + \left(\frac{\partial R}{\partial x_n}\right)^2 w_{x_n}{}^2}$ [29].

Where $R = f(x_1, x_2, x_3 \ldots x_n)$, w_R is the uncertainty in R, w_{x_n} is the uncertainty in x_n and $\frac{\partial R}{\partial x_n}$ is the partial derivative with respect to x_n.

Table E.1 shows the partial derivates used herein. The uncertainty of the tip speed ratio for all cases, $(w\lambda) \leq \pm.009$ and can therefore be neglected. Figure E.1 and Figure E.2 show the uncertainty bars applied to the averages of $C_p$and C_T for both the free tip and ducted cases. The uncertainties are fairly small, much smaller than the repeatability of the data.

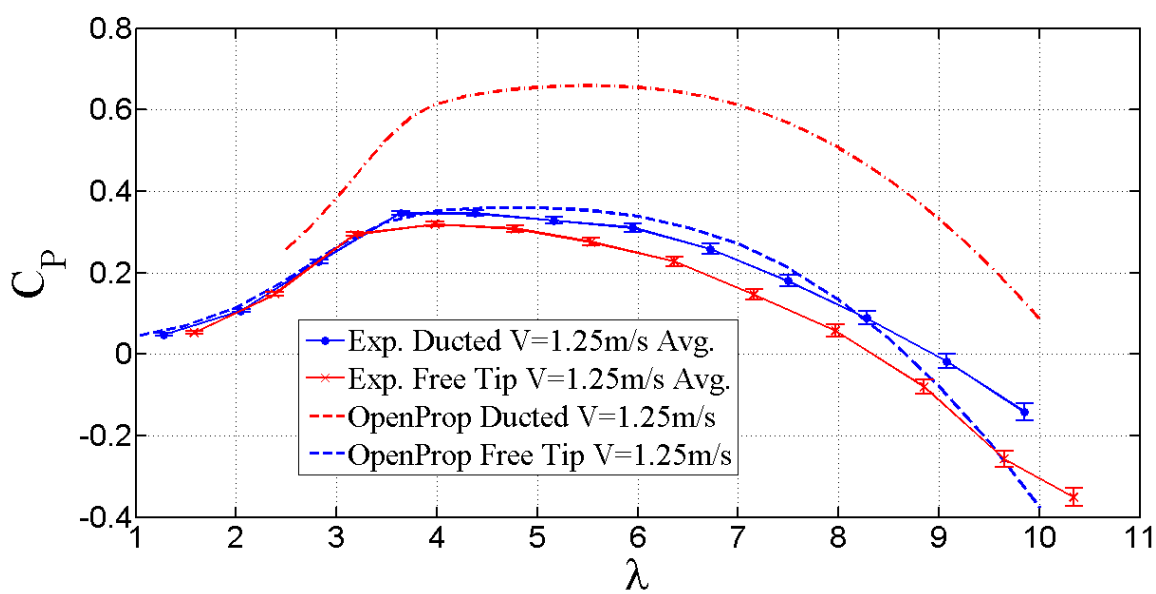

Figure E.1 Shows the uncertainty in C_p for the free tip and ducted turbines.

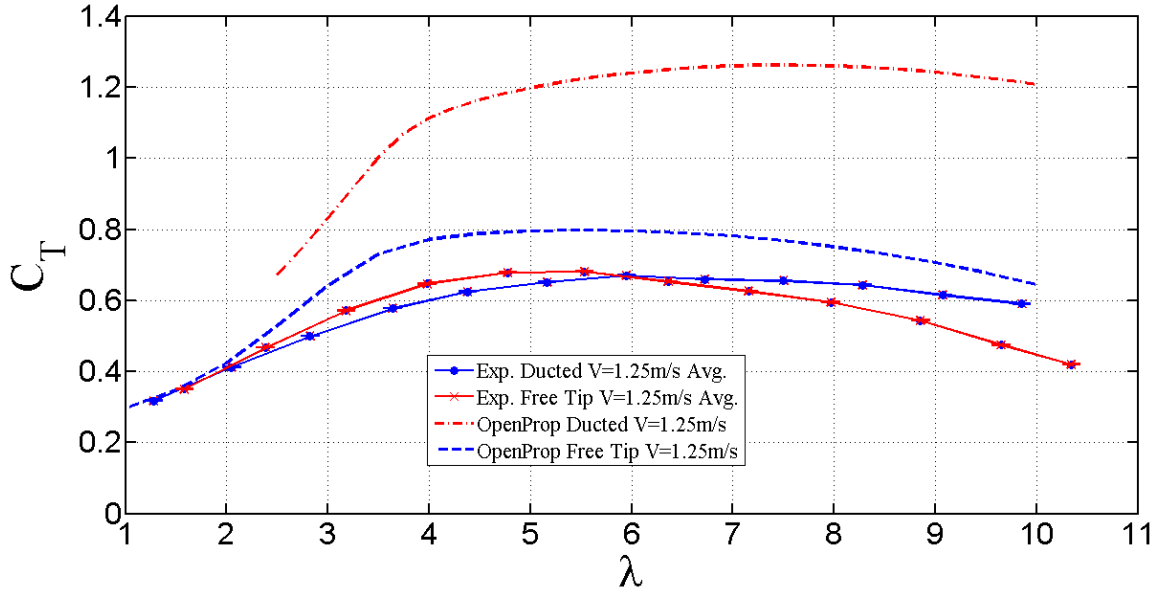

Figure E.2 Shows the uncertainty in C_T for the free tip and ducted turbines.

Table E.1 Uncertainty Equations

Partial differential equation	Equation variables in MATLAB
$C_P = \dfrac{Flw}{\frac{1}{2} r V_S^3 p \frac{D^2}{4}}$	$Cp_av = \dfrac{(avg_F)\,l\,(avg_omega)}{.5(rho)(avg_v)^3 .25(pi)D^2}$
$\dfrac{\P C_P}{\P F} = \dfrac{lw}{\frac{1}{2} r V_S^3 p \frac{D^2}{4}} = \dfrac{8lw}{r V_S^3 p D^2}$	$part_F = \dfrac{l\,(avg_omega)}{.5(rho)(avg_v)^3 .25(pi)D^2}$
$\dfrac{\P C_P}{\P l} = \dfrac{Fw}{\frac{1}{2} r V_S^3 p \frac{D^2}{4}} = \dfrac{8Fw}{r V_S^3 p D^2}$	$part_l = \dfrac{(avg_F)(avg_omega)}{.5(rho)(avg_v)^3 .25(pi)D^2}$
$\dfrac{\P C_P}{\P w} = \dfrac{Fl}{\frac{1}{2} r V_S^3 p \frac{D^2}{4}} = \dfrac{8Fl}{r V_S^3 p D^2}$	$part_omega = \dfrac{(avg_F)\,l}{.5(rho)(avg_v)^3 .25(pi)D^2}$
$\dfrac{\P C_P}{\P dx} = \dfrac{-3Flw}{\frac{1}{2} r V_S^3 dx p \frac{D^2}{4}} = \dfrac{-24Flw}{r V_S^3 dx p D^2}$	$part_dx = \dfrac{3(avg_F)\,l\,(avg_omega)}{.5(rho)(avg_v)^3 (dx).25(pi)D^2}$
$\dfrac{\P C_P}{\P D} = \dfrac{-2Flw}{\frac{1}{2} r V_S^3 p \frac{D^3}{4}} = \dfrac{-16Flw}{r V_S^3 p D^3}$	$part_D = \dfrac{2(avg_F)\,l\,(avg_omega)}{.5(rho)(avg_v)^3 .25(pi)D^3}$

Repeatability (Δ) was found by taking difference of the maximum and minimum values to the mean value of the data.

APPENDIX F: TIP GAP STUDY

Introduction

Maintaining sufficient tip gap is important to prevent interference between the blades and duct. This tip gap study will be used to answer the question of how much gap is allowable without adverse affect of ducted turbine performance.

This research is accomplished experimentally in the UMaine tow tank using the same test platform, data acquisition system, duct and rotor as previously described in this thesis. By varying the tip gap over a range of tip speed ratios a $C_p$curve was obtained for each tip gap ratio. The results are plotted with the results from the minimum tip gap for comparison purposes.

The theory behind the affects of tip gap is the subject of numerous papers and theses and is beyond the scope of this study [30][25].

Experimental Setup

After the duct and rotor were assembled and aligned to ensure the rotor was concentric to the hub, the blade tips were "ground in" to the duct to ensure an even tip clearance. This was done using emery cloth laid on the duct and turning the rotor by hand on its shaft. The tip gap was adjusted using feeler gauges and sliding the rotor in or out of the duct to achieve the desired clearance (Figure F.1).

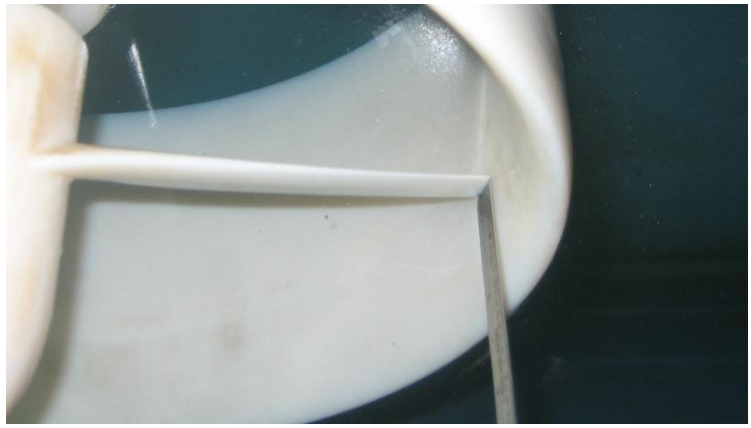

Figure F.1 Measuring tip gap on ducted turbine.

This method is reasonably accurate in terms of the tip gap but ideally one would manufacture a series of rotors each with different blade lengths. For this work fabricating three rotors was prohibitively expensive. The problem with using one rotor is that as the rotor is moved out of the duct to increase the tip gap it also changes its chordwise position along the duct. The duct rotor combination was designed in OpenProp at the ¼ chord of the duct, the affect of this change in position is not expected to be significant because the change in circulation along the relatively small change in position (approximately 2.5% of the duct length) is not significant.

Results

Based on published data [2] [31] [32] [19] 3 tip gaps ratios were chosen to test $\frac{t_g}{D} = 0.00197;\ \ 0.0039;\ \ 0.0059$. The experimental C_p curves are shown in Figure F.2 Cp as a function of t/D (V = 1.25 m/s)

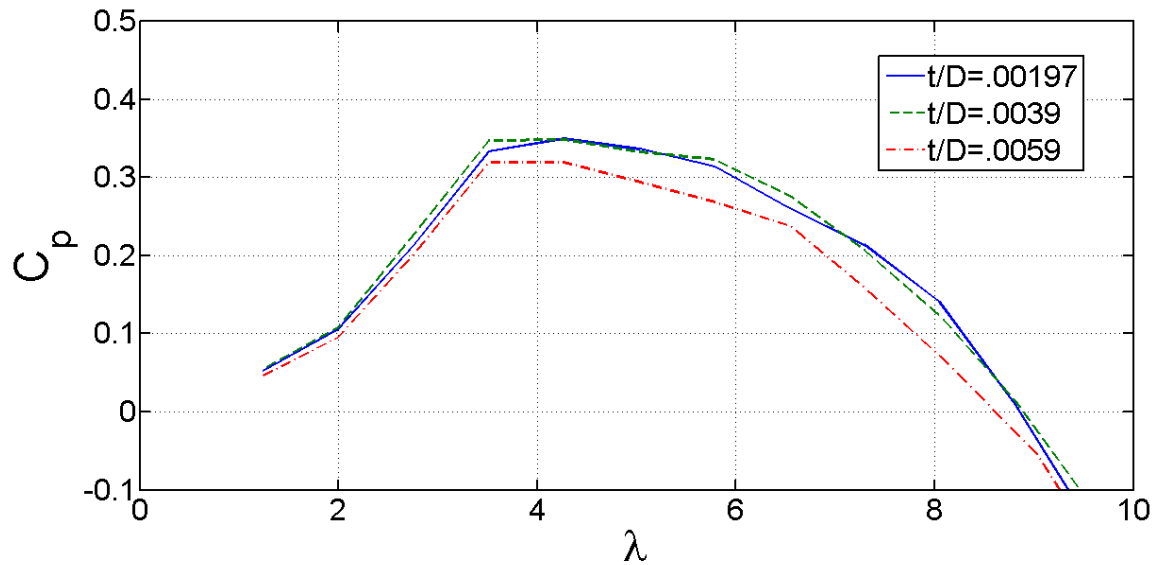

Figure F.2 Cp as a function of t/D (V = 1.25 m/s)

For the remainder of this study we will define the following cases as follows in Table F.1 Tip Gap Case Definitions.

Table F.1 Tip Gap Case Definitions

Case #1	Percent Difference between t/D = .00197 and t/D = .0039
Case #2	Percent Difference between t/D = .00197 and t/D = .0059

It was expected from previous work[2] [32] [20][19] that C_p would not change significantly for case #1 but would drop by 10% to 15% for case #2. The percent differences in C_p show that the change for case #1 varies from 0.35% to 12.5% with an average of 4.49% and the change for case #2 varies from 4.1% to 50% with an average of 14.96% (Figure F.3 Percent difference in Cp).

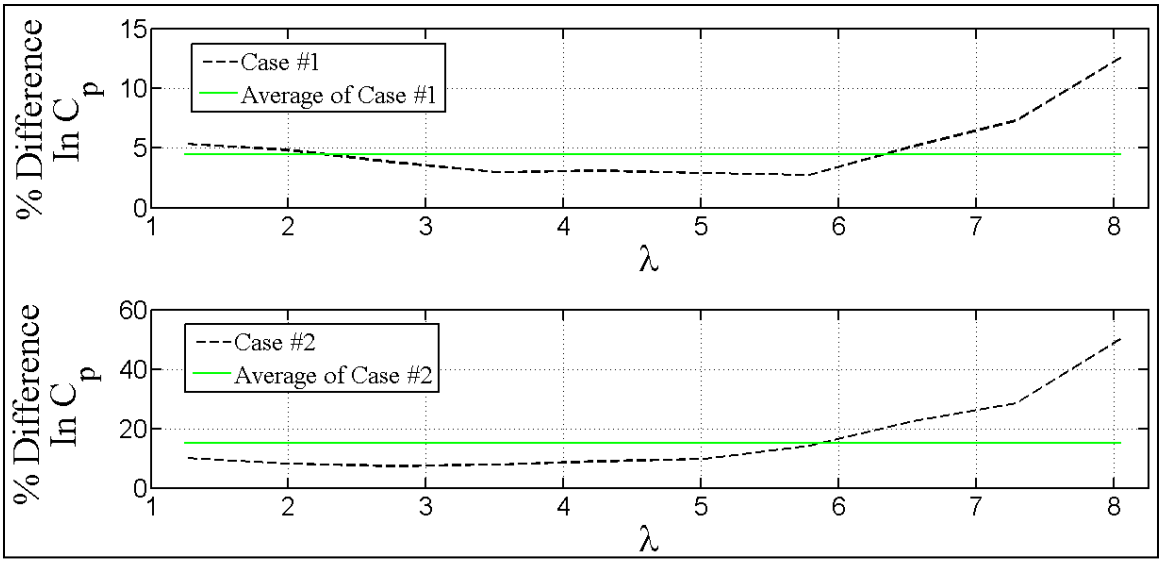

Figure F.3 Percent difference in Cp

Discussion

The results of this tip gap study are consistent with previously published experimental data on similar devices [20] [19].

<u>Case #1</u>

At first glance the experimental data in case #1 looks larger than expected with ranges of 0.35% to 12.5% variation in C_p with an average of 4.49% (Figure F.3 Percent difference in Cp) . These values in and of themselves constitute a significant change in performance but the percentages are not necessarily significant when also considering Figure F.2 Cp as a function of t/D (V = 1.25 m/s). The plot of t/D = .00197 and the plot of t/D = .0039 are identical when viewed from the standpoint of repeatability. It is clear from this plot that no trend can be ascertained, this in turn makes the percent difference in case #1 insignificant.

Case #2

Unlike case #1 (Figure F.2 Cp as a function of t/D (V = 1.25 m/s) clearly demonstrates a lower trend in C_p with increased tip gap. As predicted the experimental average of 14.96% difference in C_p falls within the expected range of 10% to 15%.

Conclusion

The experimental data shows that maintaining t/D ≤ .0039 does not significantly degrade the quality of the data in comparison to the tighter tolerance of t/D ≤ .00197.

APPENDIX G: FREE TIP TURBINE PICTURE

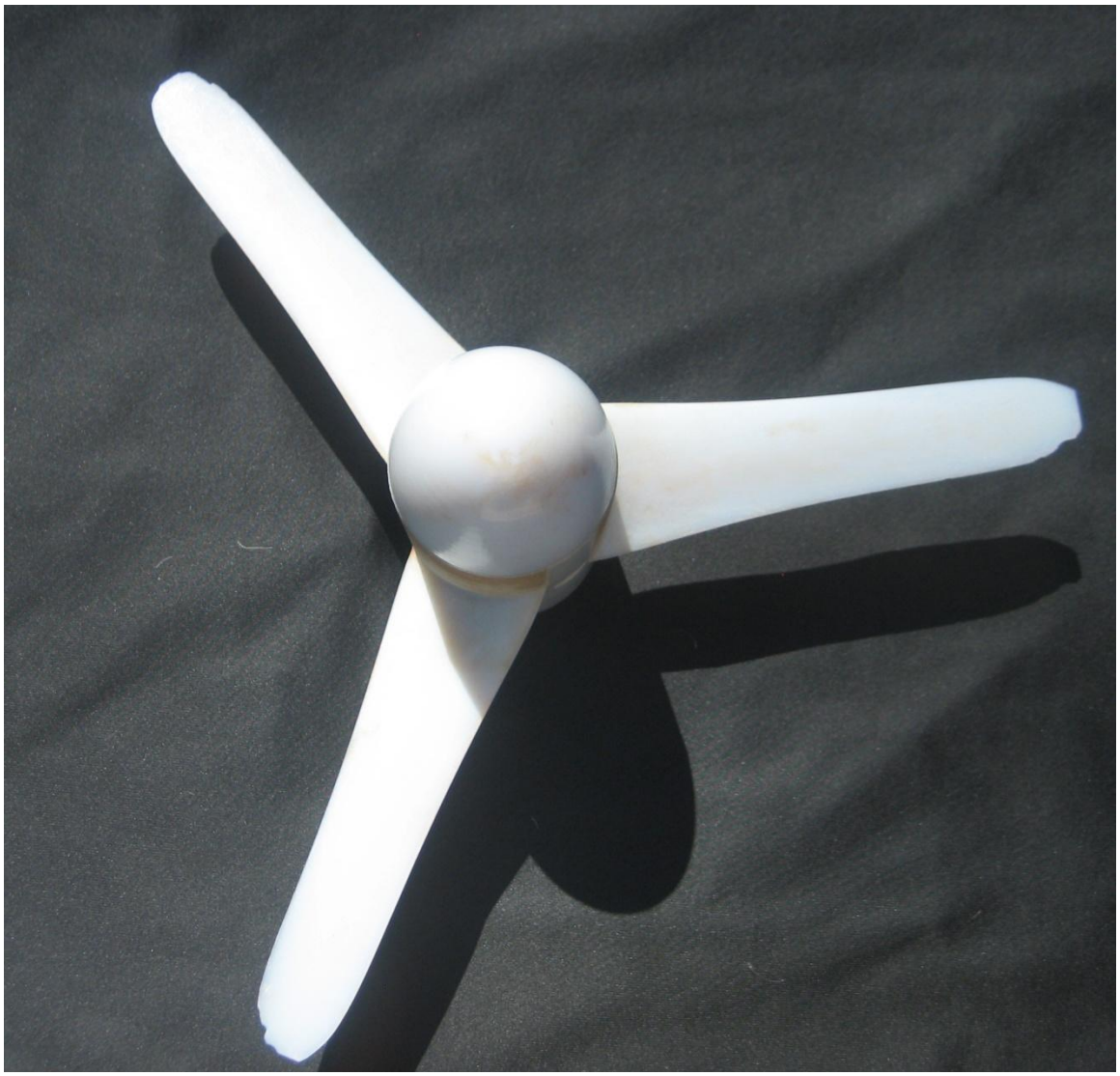

Figure G.1 Picture of the free tip turbine. Note the damaged blade tips.

BIOGRAPHY OF THE AUTHOR

Thomas A Lokocz graduated from the University of Maine in 2010 with a B.S in Mechanical Engineering. He spent several years prior to college working as a professional sailor, boat builder and yacht designer. Tom plans to pursue a career in engineering and continue living in Maine with his wife and son. Tom is a candidate for the Master of Science degree in Mechanical Engineering from the University of Maine in August, 2012.